Katharina Schwaiger, BSc

Optimization of Triacylglycerol Synthesis in Yeast

MASTER'S THESIS

to achieve the university degree of

Master of Science

Master's degree programme: Biochemistry and Molecular Biomedical Sciences

submitted to

Graz University of Technology

Supervisor

Assoc. Prof. Dr. Klaus Natter

Institute of Molecular Biosciences,
University of Graz

Graz, March 2018

This document is set in Palatino, compiled with pdfLaTeX2e and `Biber`.

The LaTeX template from Karl Voit is based on KOMA script and can be found online:
https://github.com/novoid/LaTeX-KOMA-template

Affidavit

I declare that I have authored this thesis independently, that I have not used other than the declared sources/resources, and that I have explicitly indicated all material which has been quoted either literally or by content from the sources used. The text document uploaded to TUGRAZonline is identical to the present master‘s thesis.

Date	Signature

Abstract

The improvement of lipid accumulation in yeast as microbial factories is of great interest for second and third generation biodiesel production. In order to ensure a highly efficient fermentation to triacylglycerol (TAG), specific genetic modifications of *Saccharomyces cerevisiae* were performed.

The first part focused on NADPH regeneration, as it acts as electron donor for fatty acid biosynthesis. Therefore, a recently found fungal GAPDH (klaGAPDH), which has affinity for the cofactor $NADP^+$, was introduced. Next, *UTR1*, a native NAD(H) kinase was codon optimized and overexpressed. This second metabolic intervention was performed to support the activity of klaGAPDH by increasing the availability of cytosolic $NADP^+$. Furthermore, ethanol production was suppressed by deleting the alcohol dehydrogenase gene (*ADH1*) in order to redirect the carbon flux towards TAG synthesis. The aim of these combined genetic modifications was a redox-reprogramming by shifting the NAD^+/NADH cycle via ethanol towards a $NADP^+$/NADPH cycle via fatty acid synthesis. The *klaGAPDH* mutant showed a lower ethanol excretion and a 1.5-fold increase of TAG content in comparison to the wild type. In contrast, the triple mutant most likely had to cope with redox imbalances, oxidative stress and a decelerated glycolysis resulting in a growth defect. However, these negative effects might also be derived from *UTR1* overexpression, as already the double mutant showed signs of metabolic stress. Therefore, a *klaGAPDH* adh1Δ mutant would be interesting for future investigations. In the second part of this thesis a strain bearing a mutated hexose transporter was examined regarding its glucose consumption. This mutation was designed to improve the glycolytic flux in nitrogen starved cells. The mutant showed an increased glucose uptake. However, the additionally consumed glucose was metabolized to glycogen.

The characterization of the performed genetic modifications revealed their contribution to lipid accumulation in the cell. Taking this into consideration, a highly efficient lipid-producing strain will be engineered, which may compete with oleaginous yeasts in TAG production.

Contents

Acronyms

ADH1	alcohol dehydrogenase gene
E. coli	*Escherichia coli*
GDP1opt	codon optimized NADP-GAPDH of *Kluyveromyces lactis*
PGK1	3-phosphoglycerate kinase1 gene
S. cerevisiae	*Saccharomyces cerevisiae*
TDH1	triose-phosphate dehydrogenase 1 gene
TDH2	triose-phosphate dehydrogenase 2 gene
TDH3	triose-phosphate dehydrogenase 3 gene
UTR1opt	ATP-NADH kinase gene
Y. lipolytica	*Yarrowia lipolytica*
ATP	adenosine triphosphate
C-lim	carbon limited medium
C/M 2/1	chloroform/methanol 2/1
DHAP	dihydroxyacetone phosphate
ERG	ergosterol
$FADH_2$	hydroquinone form of flavin adenosine dinucleotid
G3Pase	glycerole-3-phosphatase
GAP	glyceraldehyde 3-phosphate
GAPDH	glyceraldehyde-3-phosphate dehydrogenase
G3PD	glycerole-3-phosphate dehydrogenase
GFP	green fluorescence protein
HPLC	high performance liquid chromatography
HXT1mut	mutant hexose transporter 1 (K12,35,59R)
HXT1wt	wild type hexose transporter 1

kb	kilo base pairs
kD	kilo Dalton
klaGAPDH	glyceraldehyde-3-phosphate dehydrogenase of *Kluyveromyces lactis*
N-lim	nitrogen limited medium
NAD^+	oxidized nicotinamide adenine dinucleotide
NAD(H)-kinase	ATP-NAD(H)-kinase
NADH	reduced nicotinamide adenine dinucleotide
$NADP^+$	oxidized nicotinamide adenine dinucelotide phosphate
NADPH	reduced nicotinamide adenine dinucleotide phosphate
OD600	optical density at 600 nm
ORF	open reading frame
PCR	polymerase chain reaction
PEP	phosphoenolpyruvat
Rgt1p	glucose-responsive transcription factor
SE	sterol ester
TAG	triacylglycerol
TCA	tricarboxylic acid
TLC	thin layer chromatography
TPI	triose phosphate isomerase
YPD	yeast extract peptone dextrose

1. Introduction

1.1. Biodiesel production

Triacylglycerols (TAG) represent the source material for biodiesel production (Knothe, 2010). First generation biodiesel, esterified mainly from edible plant oils, is in competition with food industries. Plants used for biodiesel production are occupying farmland which in turn could be used for food production. This causes several economic and ethical problems. Therefore, a shift towards second and third generation biodiesel production is vital. Second generation biodiesel is manufactured from agricultural byproducts, such as wheat straw, which do not compete with food supply. A chemical treatment degrades this lignocellulosic biomass to simple sugars which can be metabolized by microorganisms (Zhang, Rodriguez, and Keasling, 2011). To ensure a highly efficient conversion to TAG, yeast metabolism has to be optimized by genetic modifications.

1.2. *Saccharomyces cerevisiae*, a non-oleaginous microorganism

In order to engineer a maximally efficient lipid-producing yeast strain, oleaginous species such as *Yarrowia lipolytica* (*Y. lipolytica*) are of great interest. All oleaginous yeasts are Crabtree negative. Under aerobic conditions they mainly generate high concentrations of biomass, CO_2 and only low amounts of ethanol. The TAG contents obtained with wild type *Y. lipolytica* are fairly high (up to 30% of biomass), but engineered species accumulate up to 90% in their biomass (Fakas, 2016).

However, one major disadvantage of oleaginous yeasts are the required high aeration rates. Especially in the production process aeration causes high costs (Yen and Liu, 2014). *Saccharomyces cerevisiae* (*S. cerevisiae*), in contrast, shows only low respiration rates, due to the Crabtree effect. Therefore, an engineered TAG producing strain might become a cost-effective alternative for oleaginous yeasts in TAG production.

Additionally, *S. cerevisiae* is one of the best studied microorganism and represents a well known model organism (Fakas, 2016). This large amount of knowledge about its metabolic processes also represents an advantage in order to perform genetic modifications.

1.3. Central carbon metabolism and lipid biosynthesis

Figure 1.1 shows an overview of the central carbon metabolism of *S. cerevisiae*. The preferred carbon source mostly is glucose, which is transported into the cell by hexose transporters. The major part enters glycolysis. The remaining glucose is stored within glycogen and trehalose or is incorporated into the cell wall in the form of glucan. Some of the glucose-6-phosphate, produced in the first step of glycolysis, enters the pentose phosphate pathway. Two molecules NADPH are generated, representing the main source of cytosolic NADPH.

During glycolysis two molecules pyruvate, two adenosine triphosphate (ATP) and two NADPH are produced out of one molecule glucose. Under respiratory conditions pyruvate is transported into mitochondria where it is converted to acetyl-CoA by oxidative decarboxylation. Next, it gets degraded via the tricarboxylic acid (TCA) cycle. Four molecules NADH, one $FADH_2$ and one ATP are produced. Subsequently, ATP is generated by the respiratory chain, where NADH and $FADH_2$ get reoxidized. L-glutamate is built from α-ketoglutarate, an intermediate of the TCA cycle, whereby one NADPH is consumed. L-glutamate acts as the nitrogen donor for the synthesis of nitrogen containing molecules, such as amino acids.

S. cerevisiae mostly produces its energy by glycolysis and fermentation to ethanol even under aerobic conditions caused by the Crabtree effect. Pyruvate in the cytosol is converted to acetaldehyde, which gets further reduced to ethanol (release of NAD^+) or oxidized to acetate (release of NAD(P)H). Acetyl-CoA is built from cytosolic acetate and represents the precursor for fatty acid-, amino acid and ergosterol synthesis. In addition mitochondrial acetyl-CoA, formed via oxidative decarboxylation, can be transported to the cytosol, where it is available again for fatty acid synthesis and TAG production (Wiebe et al., 2008).

TAG contains three fatty acids, therefore, the aim of this thesis is to stimulate fatty acid synthesis (figure 1.2). The first step requires one molecule of ATP and CO_2 for the conversion of acetyl-CoA to malonyl-CoA. This reaction is catalyzed by acetyl-CoA carboxylase (Acc1p). Malonyl-CoA serves as C2-carbon donor and reacts with acetyl-CoA to keto-acyl ACP. The acyl-carrier-protein (ACP) domain is part of the fatty acid synthase complex (Fas1p, Fas2p). The growing fatty acid is connected to the FAS complex by ACP. Three more reaction steps lead to fatty-acyl ACP, which can be used for chain elongation via the reaction with malonyl-CoA. The two reduction steps (keto acyl-ACP to hydroxy acyl-ACP and enoyl-ACP to fatty acyl-ACP) require NADPH as the reducing cofactor (Tehlivets, Scheuringer, and Kohlwein, 2007). Synthesis of palmitic acid (C16:0), for instance, oxidizes 14 NADPH molecules. Therefore, the generation of cytosolic NADPH increases the availability for fatty acid synthesis, which might trigger TAG production.

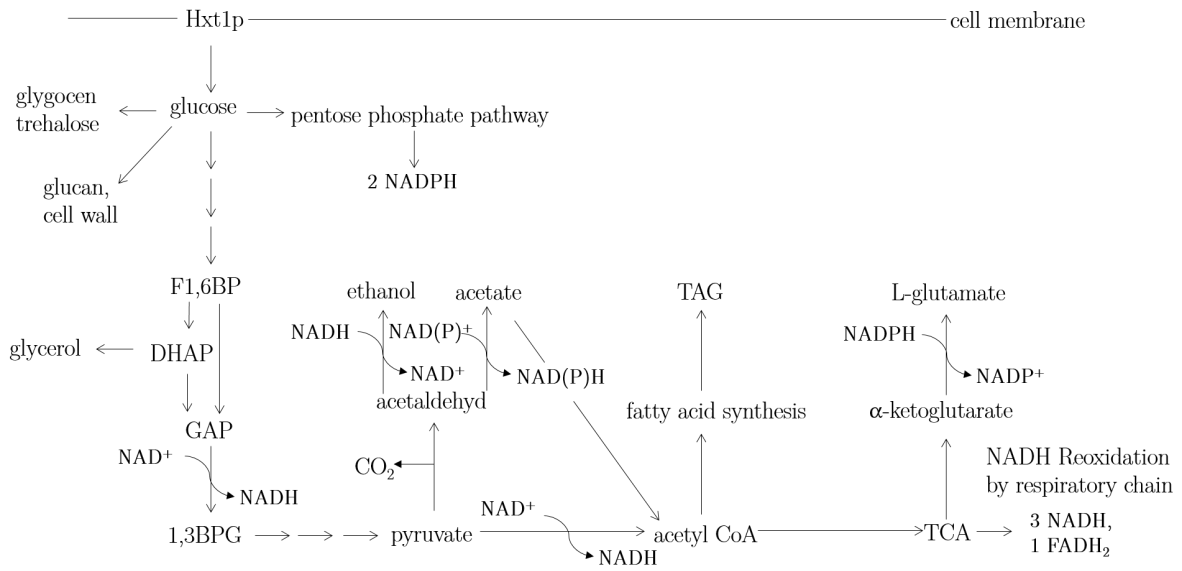

Figure 1.1.: **Central carbon metabolism**: **F1,6BP** fructose-1,6-bisphosphate, **DHAP** dihydroxyacetone phosphate, **GAP** glyceraldehyde 3-phosphate, **1,3BPG** 1,3-bisphosphoglycerate.

1.4. Metabolic interventions

The first genetic modification addresses the glycolytic glyceraldehyde-3-phosphate dehydrogenase (GAPDH), which oxidizes glyceraldehyde 3-phosphate (GAP) to 1,3-bisphosphoglycerate (1,3BPG) by utilizing one NAD^+ molecule. In order to achieve a shift of cytosolic NADH towards NADPH, the introduction of glyceraldehyde-3-phosphate dehydrogenase of *Kluyveromyces lactis* (klaGAPDH) was performed. Verho et al., 2002, found that this special form of GAPDH has affinity for both cofactors, NAD^+(K_M 500±60 μM) and $NADP^+$ (K_M 400 ± 100 μM). klaGAPDH is encoded by *GDP1*, which was codon optimized for *S. cerevisiae* and integrated into the *TDH3* locus. *TDH3* represents one native GAPDH gene of *S. cerevisiae*, which thereby was deleted.

For a more effective production of NADPH by klaGAPDH, a codon optimized and overexpressed *UTR1* represents the second intervention. *UTR1* encodes the native NAD(H)-kinase of *S. cerevisiae*, which phosphorylates NAD^+ (K_M 0.5 mM) as well as NADH (K_M 3.9 mM). Kawai et al., 2001, revealed that Utr1p consists of six identical subunits, each with a molecular weight of 60 kD. The target locus for its integration was chosen to be *TDH2*, the second native GAPDH gene. The deletion of *TDH2* might be beneficial for an effective shift towards NADPH production, as the expression of *TDH2* contributes to the cytosolic NADH amount. The overexpression of *UTR1* was performed to increase the $NADP^+$ concentration, to further maximize its availability for klaGAPDH.

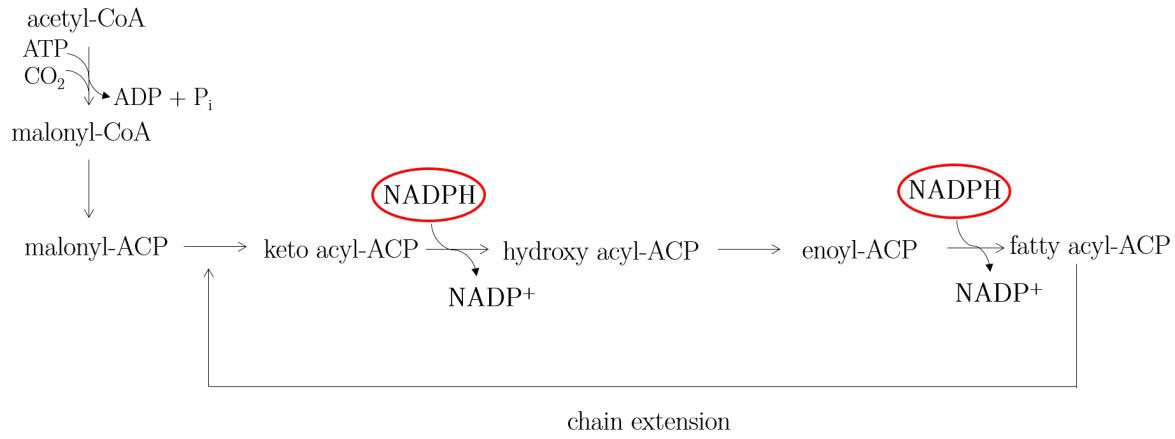

Figure 1.2.: ***De novo* fatty acid synthesis** in *S. cerevisiae*, **ACP** acyl carrier protein.

Finally, the deletion of the gene coding for the major alcohol dehydrogenase, *ADH1*, was performed. The alcohol dehydrogenase catalyzes the formation of ethanol via the reduction of acetaldehyde. NADH, produced during glycolysis, is reoxidized to be again available for glycolytic ATP production. The Crabtree positive yeast *S. cerevisiae*, mostly produces ethanol to maintain its redox balance. The intended effect of this deletion was to totally redirect carbon flux from ethanol towards TAG production.

The focus of the second part was set on a mutated hexose transporter (Hxt1p) in order to improve glucose uptake. Especially nitrogen starved cells start to accumulate lipid (Kolouchová et al., 2016). However, nitrogen limitation also triggers protein degradation, which causes a slower glucose uptake. *HXT1* was mutated by exchanging its putative ubiquitination sites (K12,35,59R) in order to prevent its degradation (Nijland et al., 2016). The overexpression of the mutated *HXT1* might enable the cell to improve glucose uptake and productivity.

In figure 1.3 all of the above described metabolic interventions are marked in the previously shown overview. In contrast to the *HXT1* mutation, the first three genetic modifications are combined in one strain.

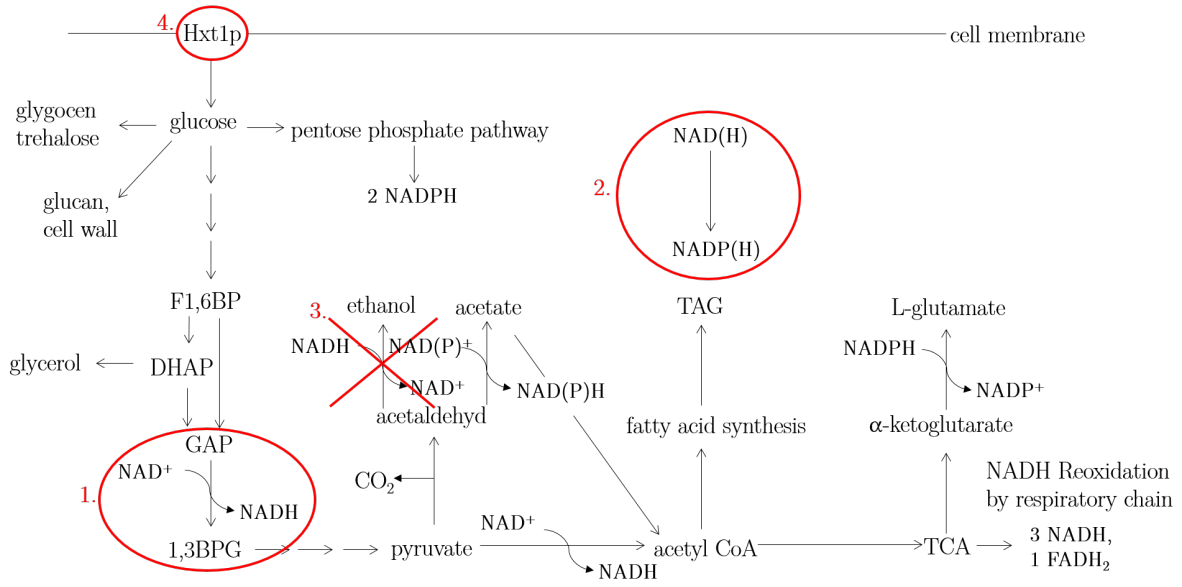

Figure 1.3.: **Metabolic interventions**: 1. klaGAPDH (*GDP1*), 2. NAD(H)-kinase (*UTR1*), 3. *ADH1* deletion, 4. mutated *HXT1*.

2. Aim of the Study

The aim of the study was to reprogram the central carbon metabolism of the Crabtree positive yeast *S. cerevisiae* in order to achieve high TAG contents.

TAG production requires NADPH as the cofactor for fatty acid synthesis. Therefore, the integration of *klaGAPDH* and *UTR1opt* was performed. NAD^+ is phosphorylated by Utr1p (NAD(H)-kinase) and $NADP^+$ gets reduced by klaGAPDH via glycolysis. The resulting NADPH acts as the electron donor in fatty acid synthesis. Ethanol production, in contrast, reoxidizes NADH, produced via glycolysis. The higher NADPH/NADH ratio might lead to a lower ethanol excretion, as less cytosolic NADH has to be oxidized, and higher TAG contents. A reinforcement of this effect was attempted by deleting *ADH1*. These metabolic interventions in combination lead to a redox-reprogramming, particularly by partially switching from a predominant NAD^+/NADH cycle to a $NADP^+$/NADPH cycle.

The last metabolic intervention represents a mutated *HXT1*. The aim was to trigger productivity by an improved glucose uptake during nitrogen limitation. A high productivity is important in order to be competitive with oleaginous yeasts regarding the produced TAG amounts.

3. Materials and Methods

In this chapter the methods and tools used during this thesis are described. A detailed list of medium compositions and chemicals can be found in the Appendix. Used buffers are stated in the respective sections.

3.1. Cloning strategies

In table 3.1 primers used for the following cloning strategies are listed.

3.1.1. *klaGAPDH* mutant

GDP1 encodes the NADP-GAPDH of *Kluyveromyces lactis*. A codon optimized version of *GDP1* was integrated into the *TDH3* locus of *S. cerevisiae* by the CRISPR/Cas9 approach (Ran et al., 2013). This was carried out by a site-directed double strand breakage (chromosome VII 882793). The down- and upstream homologous regions of the insert DNA were designed to allow for repair of this break by homologous recombination. The executing enzyme, Cas9, was encoded on pCRISPR/TDH3. Finally, the cell's own repair mechanism was recruited to fulfill the integration by homologous recombination.

The plasmid pCRISPR/TDH3 was cloned according to the NEB Gibson Assembly manual. The plasmid pCRISPR (in-house plasmid, E543) was digested with *Not*I and alkaline phosphatase. Complementary oligonucleotides (recsite_gRNA_f and recsite_gRNA_r, table 3.1) containing the gRNA (guide RNA) recognition site 5'-ACACACATAAACAAACAAAA-3' and 30 base pair overhangs, to bind the respective plasmid ends, were designed. 5 μL of an equimolar mixture, containing the digested pCRISPR and the previously annealed oligonucleotides, were added to 15 μL of the Gibson assembly master mix and incubated at 50 °C for one hour. Thereafter, the mixture was dialyzed and directly used for *Escherichia coli* (*E. coli*) transformation (see 3.3). The replicated plasmid pCRISPR/TDH3 (figure 3.1) was preparated by PureYield Plasmid Miniprep System Protocol (Promega) and sequenced (LGC Genomics).

The insert DNA was amplified from pHEY_GAPDHopt (in-house plasmid, E544) using insert_GAPDH_f and insert_GAPDH_r (table 3.1) as primers. Their sequence also

Primer ID	**Primer sequence 5' - 3'**
recsite_gRNA_f	CTTCTCCGCAGTGAAAGATAAATGATCACACACATAAACAAACAAAAGTTTTAGAGCTAGAAATAGCAAGTTAAAATAAG
recsite_gRNA_r	CTTATTTTAACTTGCTATTTCTAGCTCTAAAACTTTTGTTTGTTTATGTGTGTGATCATTTATCTTTCACTGCGGAGAAG
insert_GAPDH_f	GTTTTAAAACACCAAGAACTTAGTTTCGAATAAACACACATAAACAAACAAAATGCATCATCACCACCACCATCCAGATATG
insert_CYCT_r	CATGACCAATCTACCGATTCTACCGAAACCGTTAATAGCAACTCTAACCACGAGCGTCCCAAAACCTTCTCAAGC
TDH3_Pro_F	GTGAACAGTTTATTCCTGGCATCCAC
TDH3_ORF_R	GATACCAGCGGAAGCATCGAAG
TDH3_Pro_Seq_F	GTTGAAACCAGTTCCCTGAAATTATTC
GAPDH_control_ r	GTGGGACAATGGAATGTGAGCGGAG
CycT_ctrl_R	GCTTGAGAAGGTTTTGGGACGC
TDH3_del_R	CCGATTCTACCGAAACCGTTAATAGCAACTCTAACCGCATTTTGTTTGTTTATGTTTATTCGAAACTAAGTTCTTGG
TDH3_del_F	CCAAGAACTTAGTTTCGAATAAACATAAACAAACAAAATGCGGTTAGAGTTGCTATTAACGGTTTCGGTAGAATCGG
UTR1_pHEY2_A1	GAATTCGACGTCGTCGACGGTACCCAGCTGATGCATCATCACCACCACCATAAGGAAAAC
UTR1_pHEY2_C	CATGATGCGGCCCTCTAGATGCATGCGGATCCTTAAACAGAGAATCTAGCTTGGGATGGCTTTG
pHEYg1_HXT7_f	CGAAGTTATCCCATCCCCGGGACTAGTGCCCTCGTAGGAACAATTTCGGGCC
pHEYg1_UTR1_r	CATGATGCGGCCCTCTAGATGCATGCGGATCTTAAACAGAGAATCTAGCTTGGGATGG
UTR1_ctrl_R	CAAGACGGTACCGTCACCACC
TDH2_ctrl_R	CAATGTTTAGAGAAGCCCATGGC
HXT7_ctrl_F	CCCCACCATCTTTCGAGATCCC
CycT_seq_r	GGACCTAGACTTCAGGTTGTC
UTR_seq3'_fwd	CTGTCCACATGCTTTGTCTTTCAG
kan_fwd	CTTGTCATTTGTATAGTTTTTTTATATTGTAG
seq_kan	GTAATATCATGCGTCAATCGTATGTG
recsite_ADH1_f	GAAACTTCTCCGCAGTGAAAGATAAATGATCGTTATCTTCTACGAATCCCAGTTTTAGAGCTAGAAATAGCAAGTTAAAATAAG
recsite_ADH1_r	CTTATTTTAACTTGCTATTTCTAGCTCTAAAACTGGGATTCGTAGAAGATAACGATCATTTATCTTTCACTGCGGAGAAGTTTC
repADH1del_f	CAAGTCTATCCCAGAAACTCAAAAAGTGTTATCTTCTACGAATCCCATAAGTTGGAATACAAAGATATTCCAGTTCCAAAGCC
repADH1del_r	GGCTTTGGAACTGGAATATCTTTGTATTCCAACTTATGGGATTCGTAGAAGATAACACTTTTTGAGTTTCTGGGATAGACTTG
ADH1pro_ctrl_f	CAGAGCTGATGAGGGGTATCTC
ADH1ter_ctrl_r	CAGTCACCGTGCCAAGCGTG
ADH1_seq_f	GTTTCCTCGTCATTGTTCTCGTTC
HXT1_GFP_f	GACCTAATGCATGATGACCAACCATTTTACAAGAGTTTGTTTAGCAGGAAAGTGAGCAAGGGCGAGGAGC
HXT1_GFP_r	GAAATTAAATACTGTATAAGTCATTAAAATATGCATATTGAGCTTGTTTAGTTTATTAGAAAAACTCATCGAGCATCAAATG

Table 3.1.: Primer list

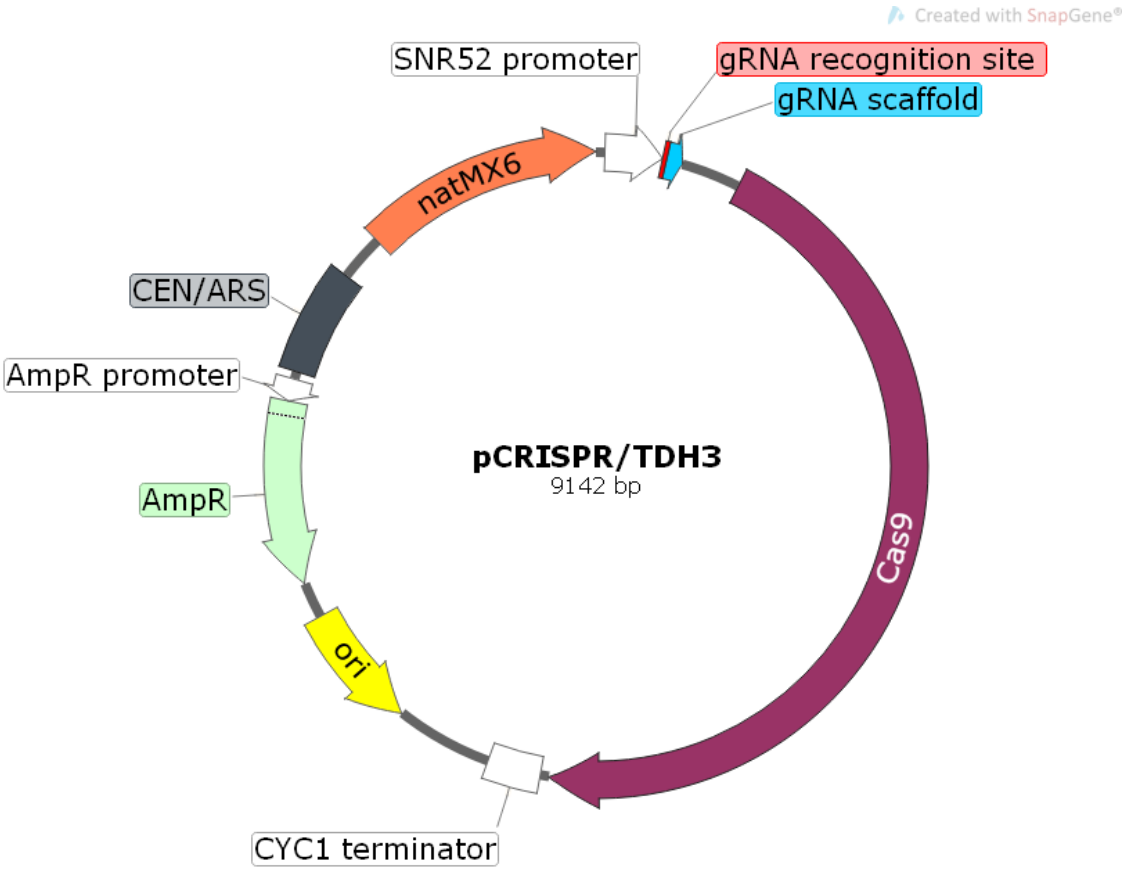

Figure 3.1.: **Map of pCRISPR/TDH3**. **SNR52 promotor** for the *S. cerevisiae* small nucleolar RNA gene SNR52, inserted **gRNA recognition site** for guiding the Cas9 to the target PAM site, **guide RNA scaffold** for the *Streptococcus pyogenes* CRISPR/Cas9 system, **Cas9** (Csn1) endonuclease from the *Streptococcus pyogenes* Type II CRISPR/Cas system, **CYC1** transcription terminator, **ori** high-copy-number origin for *E. coli* replication, **AmpR** βlactamase *E. coli* selection marker, **CEN/ARS** *S. cerevisiae CEN6* centromere fused to an autonomously replicating sequence, **natMX6** nourseothricin acetyltransferase yeast selection marker.

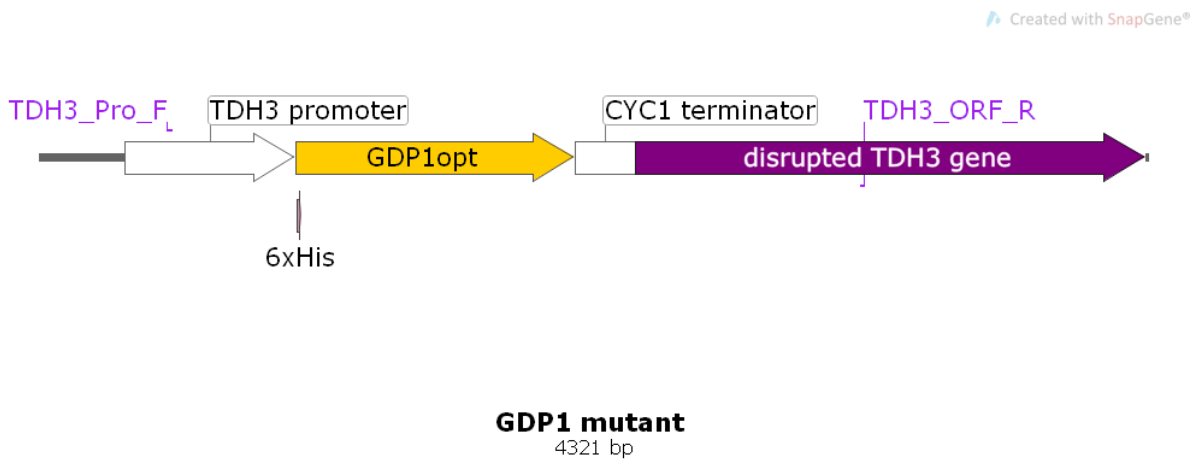

Figure 3.2.: *TDH3* locus of the *klaGAPDH* mutant: native **TDH3 promotor** of *S. cerevisiae*, 6×**His** N-terminal HIS-Tag of *klaGAPDH*, **GDP1opt** codon optimized klaGAPDH, **CYC1** transcriptional **terminator**, **disrupted TDH3** open reading frame (ORF), **TDH3_Pro_F and TDH3_ORF_R** PCR primers.

included 50 bp homologous regions to the target locus *TDH3*. The PCR was performed with Herculase II DNA polymerase. After amplification, the PCR mixture was incubated with *Dpn*I to digest the template plasmid pHEY_GAPDHopt. Subsequently, the PCR product was purified using the Wizard SV PCR Clean-Up System (Promega). 500 ng of the pCRISPR/TDH3 and 5 μg of the purified insert (1422 bp) were used for the high efficiency cotransformation of CEN.PK 113-7D wild type strain.

The genomic DNA of some colonies, which were grown on nurseothricin containing YPD plates, was isolated as described in section 3.1.6. The *TDH3* locus was amplified to select putative positive mutants. TDH3_Pro_F and TDH3_ORF_R were used as primers for the PCR. The amplified DNA fragments showing the correct basepair lenth were purified from an agarose gel using the Wizard SV Gel Clean-Up System (Pomega) and the whole *GDP1opt* cassette including upstream and downstream regions, belonging to the *TDH3* locus, was sequenced (TDH3_Pro_Seq_F, CycT_ctrl_R, tabe 3.1, 3.2).

3.1.2. *tdh3*Δ mutant

The *TDH3* deletion was carried out again using the plasmid pCRISPR/TDH3 (figure 3.1) to ensure a site-directed DNA breakage performed by the Cas9 enzyme. Complementary oligonucleotides (TDH3_del_R, TDH3_del_F, table 3.1) were designed, bearing up- and downstream homologous regions similar to those used for the integration of the *GDP1opt* cassette. Within these oligonucleotides a reading frame shift was introduced to the *TDH3* open reading frame (ORF). The insertion of two more nucleotides for *TDH3* deletion was confirmed by sequencing using the primer TDH3_Pro_Seq_F (table 3.1).

3.1.3. *klaGAPDH UTR1* mutant

The *klaGAPDH* mutant was used for the integration of the codon optimized *UTR1opt*. This was performed by exchanging the full length native *TDH2* with the *UTR1opt* cassette (HXT7 promoter, *UTR1opt*, CYC1 terminator). Instead of using the CRISPR/Cas9 system, a linear DNA fragment consisting of the kanMX cassette (TEF promoter, KanR, TEF terminator) as the selectable marker and the *UTR1opt* cassette, was transformed. The linear DNA fragment was flanked by the respective down- and upstream homologous regions for integration into the *TDH2* locus.

First, a N-terminally HIS-tagged codon optimized version of *UTR1opt* was ordered at Eurofins Genomics. The codon optimization was performed using DAMBE software. *CDC19* and *TDH3* served as reference genes. The *UTR1opt* was delivered within the plasmid pEX-K4_UTR1opt, which was transformed into *E. coli*. After comfirming the correctness of the replicated plasmid by a restriction digest, the respective strain was stored at −75 °C. Next, *UTR1opt* was cloned into the plasmid pHEY_2 to combine it with a strong promoter (HXT7) and a terminator (CYC1). The amplification of the *UTR1opt* was done with Herculase II DNA Polymerase using the primers UTR1_pHEY2_A1 and UTR1_pHEY2_C (table 3.1), each bearing 30 bp overhangs for the subsequent Gibson assembly. The PCR product was purified from an agarose gel, similar to the *Not*I digested pHEY_2. Cloning was performed by Gibson assembly resulting in the sequence confirmed pHEY_2_UTR1 (figure 3.3).

Thereafter, the *UTR1opt* cassette was cloned into the plasmid pHEYg1 to get a yeast selectable marker attached. The plasmid pHEY_2_UTR1 was used as a template to amplify the *UTR1opt* cassette with the respective primers pHEYg1_HXT7_f and pHEYg1_UTR1_r (table 3.1). The resulting PCR product and the purified *Nae*I and *Bam*HI digested pHEYg1 were used for the Gibson abssembly. *Nae*I, a restriction enzyme, removed the TEF promoter of the pHEYg1, as the amplified insert already contained a promoter (HXT7). Besides that, the final target strain (maxTAG, see chapter 7) bears some additional mutations, which are under control of the TEF promoter. This might cause problems regarding interactions between complementary sequence regions. However, the resulting plasmid pHEYg1_UTR1_TDH2 (figure 3.4) was sequenced and further used as a template for the final insert amplification.

Finally, the amplification of the DNA fragment consisting of the kanMX cassette, including its loxP sites, and the *UTR1opt* cassette, was carried out. The PCR was performed with the proofreading DNA polymerase Phusion and primers (TDH2Pro_KAN_f, TDH2Ter_CycT_r), which were designed to attach 50 bp of the respective down- and upstream homologous region to the PCR product. After its purification (3969 bp) from an agarose gel, 1-2 μg were used for the high efficiency transformation. The cells were plated on G418 (geniticin) plates, allowing to specifically select those bearing the kanMX cassette. A confirmation of the mutated *TDH2* locus was obtained by sequencing (Microsynth),

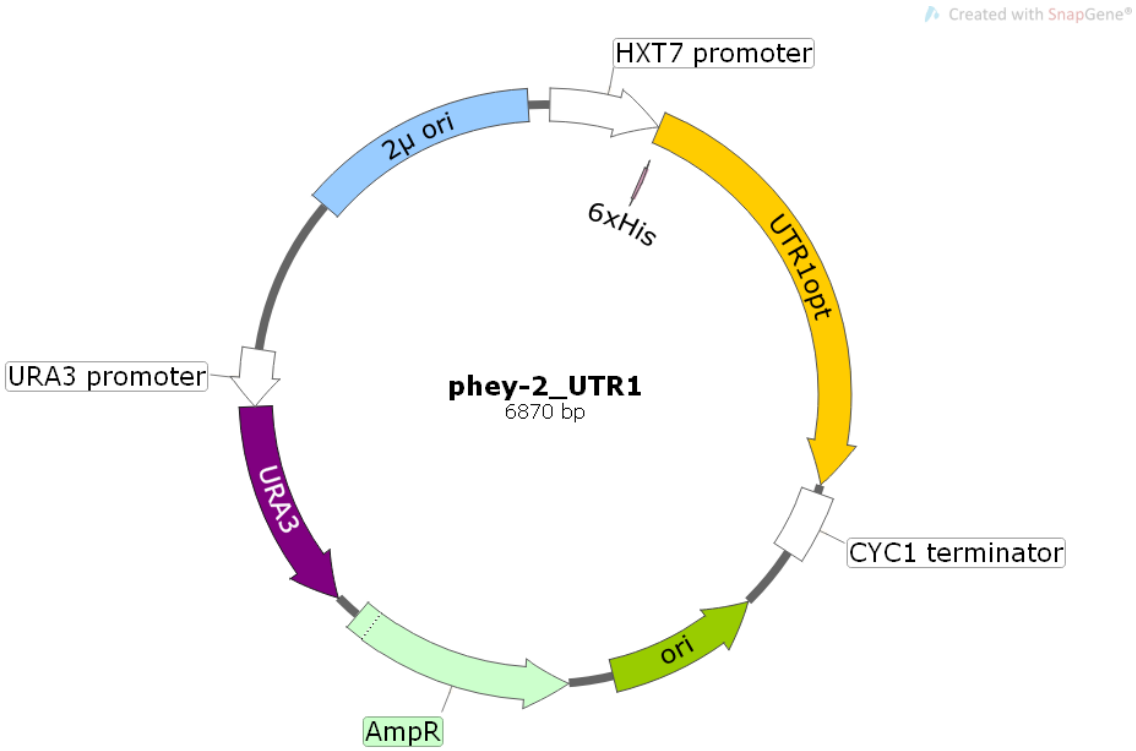

Figure 3.3.: **pHEY-2_UTR1**: **HXT7 promoter** represents a strong constitutively active promoter, **UTR1opt** codon optimized version of *UTR1* **CYC1 terminator**, **URA3** yeast auxotrophic marker required for uracil biosyntheis (orotidine-5'-phosphate decarboxylase), 2μ **ori** yeast plasmid origin of replication.

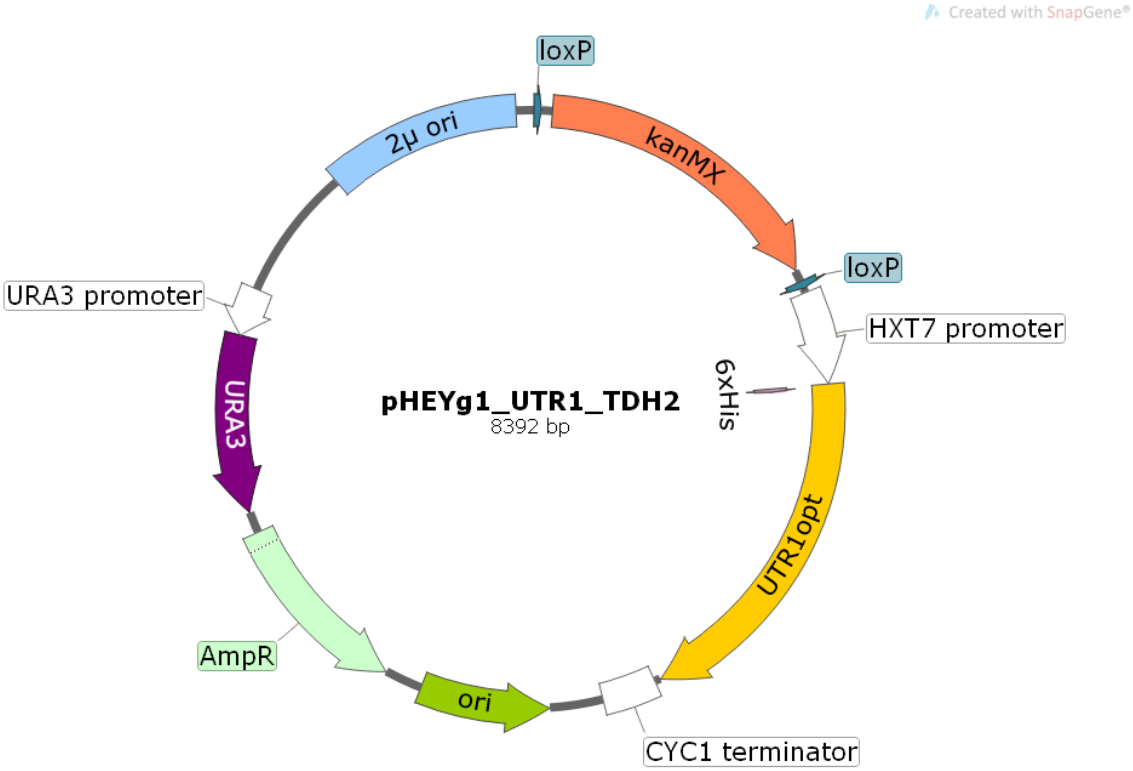

Figure 3.4.: **pHEYg1_UTR1_TDH2**: **loxP** recombination system of bacteriophage P1 for site specific deletion of kanMX, **kanMX** yeast selectable marker conferring kanamycin resistance, **UTR1opt** codon optimized *UTR1opt* flanked by **HXT7 promoter** and **CYC1 terminator**, **6xHis** N-terminal His-Tag of *UTR1opt*.

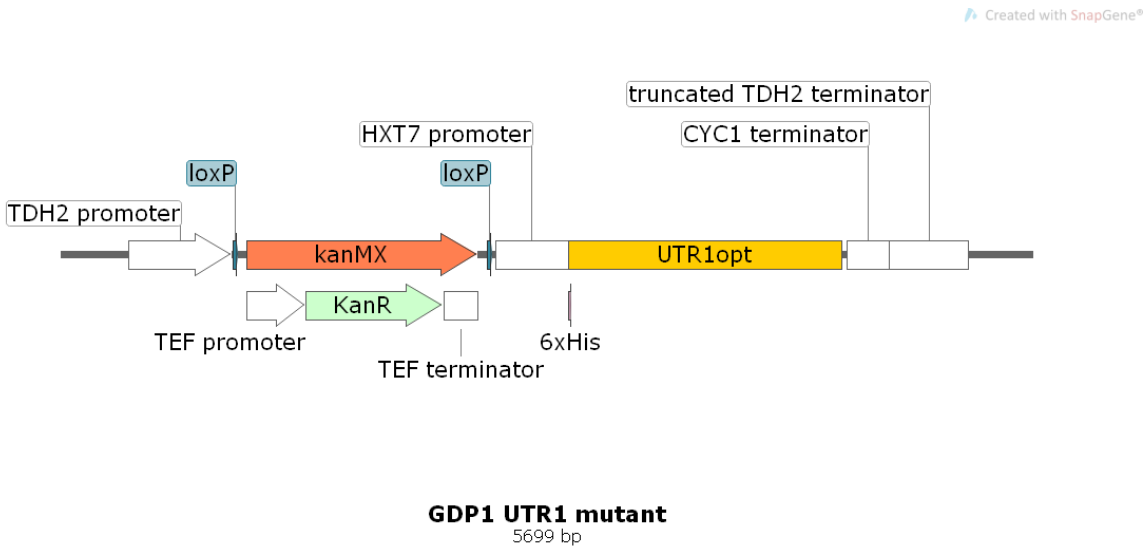

Figure 3.5.: TDH2 locus of the *klaGAPDH UTR1* mutant.

starting from the *TDH2* promoter and ending at the *TDH2* terminator (figure 3.5). This was performed by amplifying three subsequent regions of the target locus using different sequencing primers (table 3.1). The aim was to cover the whole integrated cassette. The integration was performed at chromosome X (coordinates: 454681 to 453520).

3.1.4. *klaGAPDH UTR1 adh1*Δ mutant

The third genetic modification was again performed following the CRISPR/Cas9 approach, similar to the *TDH3* deletion. The pCRISPR/ADH1 plasmid cloning was performed as described in section 3.1.1. For the Gibson assembly the complementary oligonucleotides recsite_ADH1_f and recsite_ADH1_r (table 3.1), consisting of the *ADH1* recognition site for the gRNA 5'-GTTATCTTCTACGAATCCCA-3', were used. After the plasmids sequence confirmation the transformation of the *klaGAPDH UTR1* mutant was performed. Therefore, the corresponding complementary repair oligonucleotides (repADH1del_f, repADH1del_r, table 3.1) were cotransformed. In order to achieve a reading frame shift of the *ADH1* ORF, the oligonucleotides were designed to integrate site-specifically additional nucleotides, resulting in a loss of function mutation. The mutated genomic DNA was amplified using the primers ADH1pro_ctrl_f and ADH1ter_ctrl_r, followed by sequencing (ADH1_seq_f, table 3.1).

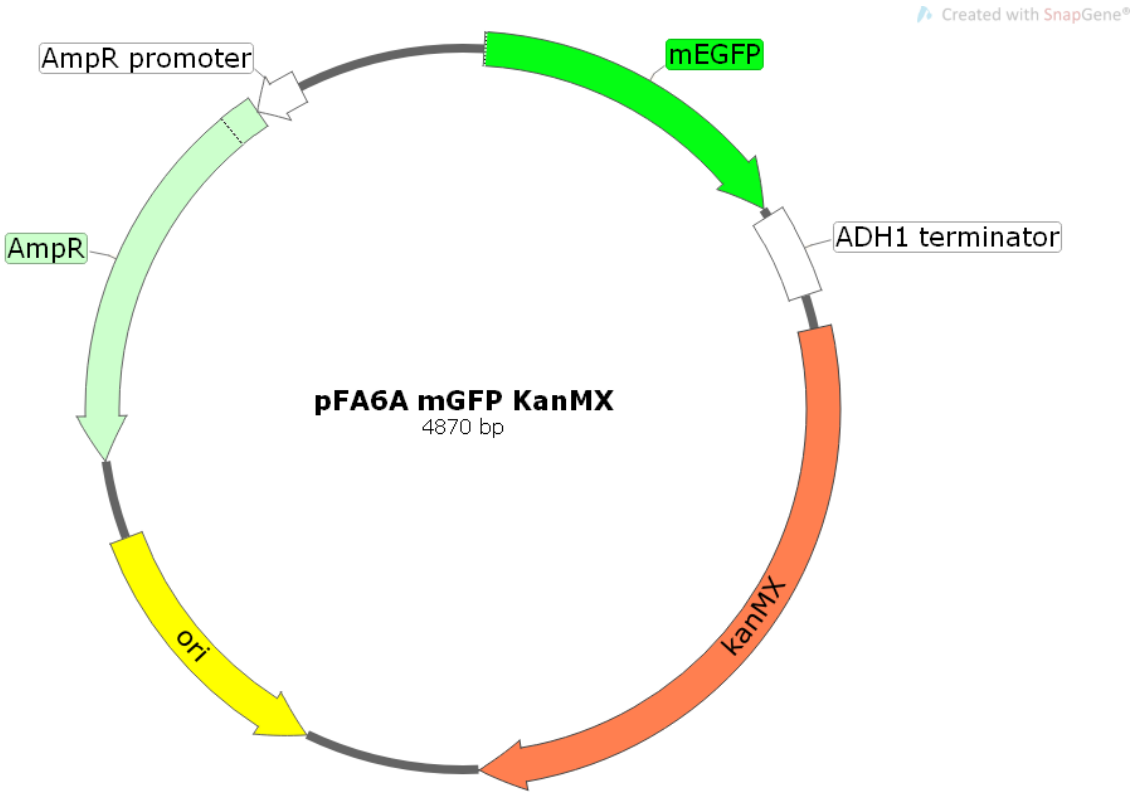

Figure 3.6.: **pFA6A mGFP KanMX: mEGFP** enhanced GFP with monomerizing A206K mutation.

3.1.5. *HXT1-GFP* mutants

The *HXT1* mutant represents a CEN.PK 113-7D strain bearing a mutated hexose transporter (Hxt1p) to prevent degradation during nitrogen starved conditions. Therefore, three lysines (K12, K35, K59) in the N-terminal region, which represent putative ubiquitination sites, were mutated to arginines according to Roy et al., 2014. Moreover, the native promoter was exchanged to *PGK1* in order to avoid control by the glucose-responsive transcription factor (Rgt1p) and to obtain overexpression.

Degradation differences were observed by tagging *HXT1mut* (mutant *HXT1*) and *HXT1wt* (wild type *HXT1*) with the green fluorescence protein (GFP). Therefore a DNA fragment consisting of the *GFP* gene, *ADH1* terminator and a kanMX cassette were amplified from the in-house plasmid pFA6A_mGFP_KanMX (figure 3.6). The primers (HXT1_GFP_f, HXT1_GFP_r) were designed to attach the respective down- and upstream overhangs, which are essential for the site-directed integration of the GFP-tag. The PCR was carried out using Phusion DNA polymerase. 1 μg of the purified PCR product was used for each transformation (*HXT1* mutant and Cen.PK113-7D). The clones were selected from G418 plates and the GFP-tag was confirmed by fluorescence microscopy.

3.1.6. Cloning methods

Isolation of genomic DNA

5 mL of overnight cultures grown in yeast extract peptone dextrose (YPD) were centrifuged for 5 minutes at 3,500 rpm. The pellet was washed with ddH_2O and resuspended in 200 μL breaking buffer (table 3.3). 200 μL glass beads and 200 μL phenol/chloroform/isoamyl alcohol were added and vortexed for three minutes. Subsequently, (table 3.2) was added and the cell lysate was mixed with 200 μL TE-buffer. The suspension was centrifuged (16,000 g, 5 minutes) and the aqueous phase was withdrawn for ethanol precipitation. 1 ml of absolute ethanol was added, mixed by inversion and centrifuged for 3 minutes. The pellet was resuspended in 400 μL TE buffer, 10 μL 4 M ammonium acetate and 1 ml absolute ethanol were added and mixed by inversion. After another centrifugation step the supernatant was removed and the tubes were left for drying at room temperature. Finally the dried pellet was resuspended in 100 μL ddH_2O and stored at $-20\,°C$.

Table 3.2.: **TE-buffer**

Tris-HCl pH 8.0	10 mM
EDTA pH 8.0	0.5 mM
ddH2O	rest

Table 3.3.: **Breaking buffer**

Triton X-100 (stock 10%)	2%
SDS (stock 20%)	1%
NaCl	100 mM
Tris-HCl pH 8.0	100 mM
EDTA pH 8.0	1 mM

Polymerase chain reaction (PCR)

PCR reactions were performed with proofreading DNA polymerases (Herculase II Fusion or Phusion) according to their respective protocols. Annealing temperatures were set between 55 °C and 65 °C depending on the respective calculated salt adjusted annealing temperatures of the primers used. These temperatures were obtained by the Oligonucleotide Properties Calculator. All PCR reaction were carried out with the thermocycler GeneAmp PCR System 9700.

E. coli transformation

4 μL of the dialyzed Gibson assembly mixture were added to 40 μL of electrocompetent *E. coli* cells. They were incubated for 20 minutes on ice and transferred to a sterile 2 mm electroporation cuvette. Electroporation was performed by setting the voltage to 2,500 V

for 5 milliseconds on the Eppendorf Multiporator. Thereafter, 700 μL of prewarmed LB (lysogeny broth) medium (table 3.4) was added and the cells were recovered for 40 minutes at 37 °C. Finally the cells were plated on ampicillin containing LB plates and put overnight at 37 °C for growing.

Table 3.4.: **LB liquid medium**

Trypton	10 g L^{-1}
Yeast extract	5 g L^{-1}
NaCl	5 g L^{-1}
ddH_2O	rest

Plasmid selection was performed by adding ampicillin (100 μg mL^{-1}) to the LB liquid medium after autoclaving and for plates 20 g L^{-1} agar was added before autoclaving.

Yeast transformation

The high efficiency transformation was performed with 5 mL YPD overnight cultures. They were inoculated in 50 mL YPD to an optical density at 600 nm (OD600) of 0.15 and incubated until they reached an OD600 of 0.6. After the cells were harvested and washed with sterile water (3,000 g, 5 minutes) the pellet was resuspended in 1 mL 100 mM lithium acetate. Subsequently, the cells were centrifuged 15 seconds at maximum speed (table top centrifuge) and the supernatant was removed. Once again the cells were resuspended in 100 mM lithium acetate to a final volume of 500 μL. 50 μL of the suspension was transferred to a new microcentrifuge tube and pelleted. After removing the supernatant 240 μl PEG 4000 (polyethylene glycol), 36 μl 1 M lithium acetate, 10 μL carrier DNA (10 mg mL^1), $1 - 5$ μg DNA (plasmid and/or linear DNA fragment) and sterile water were added to the cells. Subsequently, the suspension was incubated for 30 minutes at 30 °C followed by 30 minutes at 42 °C for the heat shock. Thereafter, the cells were microcentrifuged at 7,000 rpm for 15 seconds to remove the supernatant and $300 - 500$ μL YPD were added to recover 1-2 hours. Afterwards, the cells were washed with sterile water and plated on the respective selection plates (G418, clonNAT). The plates were incubated for two to four days to achieve an appropriate growth.

3.2. Analytical methods

3.2.1. Cultivations and growth rate analysis

Compositions of used media (C-lim, N-lim) are listed in the appendix. Cultivations were performed in the shaking incubator at 30 °C. Main cultures, used for analytical methods (lipid analysis, growth rates, western blots), were cultivated in 500 mL shake flasks filled with 100 mL medium. Precultures were cultivated overnight in 5 mL tubes carbon limited medium (C-lim) and washed with sterile water if the main cultivation was performed

in nitrogen limited medium (N-lim). Otherwise the precultures were directly used for C-lim inoculations. Cell densities were measured photometrically for N-lim cultivations, whereby main cultures were inoculated to an OD600 of 0.05. C-lim inoculation volumes were calculated by the measured preculture cell count mL^{-1} (CASY), the respective growth rates of the cultivated cells and the desired end density at a certain time point.

The determination of the dry weight was done by filtering the liquid cultures through preweighed membranes (Whatman filters, GE Healthcare). The membranes were dried overnight at 65 °C and after cooling the weight difference was measured. Cell densities were measured in a CASY TTC cell counter (Schärfe Systems, Germany) with a 60 μm capillary.

Growth rate determination was performed in C-lim and measured in CASY after overnight cultivation. Every 90 minutes the cultures were measured starting with a cell count between $1 - 4 \times 10^6$ cells mL^{-1}. In the course of the measurements the cells reached cell counts of at least 2×10^7 cells mL^{-1} or a biovolume of 1×10^9 mL^{-1}. The biovolumes were corrected conferring the respective volume loss during cultiviation caused by evaporation. The resulting biovolumes were plotted against the corresponding time points as an exponential function. The obtained exponents represented the specific growth rates of the strains. These measurements were performed with two independent biological replicates, possible changes are stated.

In parallel to every single measurement conferring growth rate determination or lipid analysis, 1 ml of culture was withdrawn, centrifuged at 12,000 rpm and the supernatant was stored at −20 °C. These samples were investigated regarding the cells excreted metabolites and incorporated glucose. The quantification was performed by an Agilent high performance liquid chromatography (HPLC) System equipped with an Aminex HPX-87H column (Biorad, Richmond, CA, USA), an Agilent autosampler, an Agilent UV detector and a Knapp RI detector. As eluent 5 mM H_2SO_4 was used. Flow rate and temperature were adjusted to 0.6 mL min^{-1} and 60 °C, respectively.

3.2.2. Lipid analysis

1×10^9 to 5×10^9 cells were harvested by centrifugation and immediately stored at −75 °C until further processing. Lipids were extracted according to a modified Folch method (1957). The frozen cell pellet was resuspended in chloroform/methanol 2/1 (C/M 2/1) and transferred to a Pyrex tube filled with glass beads. Cell disruption was achieved by shaking 30 minutes at 4 °C. Next, 1 mL 0.034% $MgCl_2$ was added before the tubes were shaken for additional 10 minutes. After centrifugation for 6 minutes at 3,000 rpm the upper aqueous phase was removed. This centrifugation step was repeated after adding an artificial upper phase ($MeOH/H_2O/CHCl_3$, 48/47/3, v/v/v) to remove the remaining water. The organic phase was collected and the glass beads left in the tubes were washed

by vortexing and centrifuging in a mixture of 2 mL C/M 2/1 and 1 mL artificial upper phase. The upper aqueous phase was again discarded and the organic phase transferred to the tube containing the organic phase from before. The pooled organic phases were mixed and evaporated under a nitrogen stream. The remaining lipids were resuspended in 1 mL C/M 2/1 and transferred to 1.5 mL sample vials and evaporated again to finally store them at −20 °C.

For lipid quantification the frozen samples were thawed and resuspended in C/M 2/1. Sample application was performed automatically by CAMAG Automatic TLC Sampler 4 (ATS4). The used silica gel plates (Merch, Germany) were put into a chamber containing the mobile phase (petrol ether/diethylether/acetic acid, 32/8/0.8, v/v/v). Lipids were separated by the rising mobile phase towards the upper end of the plates driven by the capillary effect. Afterwards, the dried plates were immersed in a solution composed of equal volumes of water and ethanol and containing 3.2% H_2SO_4 and 0.5% $MnCl_2$. Subsequently the lipids were charred for 13 minutes at 120 °C for visualization. Finally, the resulting spots were scanned at 450 nm by CAMAG TLC Scanner 3 and quantified against standards containing ergosterol (ERG), TAG and cholesteryl palmitate using CAMAG winCATS software (version 1.4.10). Each thin layer chromatography (TLC) was performed twice as a technical duplicate.

3.2.3. Protein analysis

Cytosolic fractionation

Cells grown in 500 mL C-lim in a 2 L shaking flask were harvested in late exponential phase (4×10^7 to 8×10^7 cells mL^{-1}) by centrifuging 5 minutes at 3,500 rpm. After a washing step the cell wet weight was determined, which was needed for a proper volume calculation of the following used buffers. Cell pellets were resuspended in buffer A (2 mL g^{-1}, table 3.5) with 10 mM DTT (dithiotreitol) and incubated for 10 minutes at 30 °C in the shaking incubator to prevent oxidation of the proteins thiol groups. After another centrifuging step buffer A was discarded and a washing step with buffer B (table 3.6) followed. The cells pellets were resuspended in buffer B (7 mL g^{-1}). Zymolyase (5 mg g^{-1}) was added to the cell suspensions followed by incubation for 40 minutes at 30 °C. The resulting spheroplasts were centrifuged for 5 minutes at (4 °C, 3,000 rpm) and carefully washed with buffer B. The spheroplasts were resuspended in buffer C (7 mL g^{-1}, table 3.7) and 1 mM protease inhibitor mixture (table 3.8) was added before they were disrupted in a Dounce Homogenizer using a thight fitting pestle (15x). The homogenates were centrifuged for 5 minutes at 3,500 rpm and 4 °C to remove the cell debris. Finally the supernatants were centrifuged for 45 minutes at 45,000 g and 4 °C to pellet the cell organelles. The cytosolic fraction (supernatant) was stored at −20 °C until further processing.

Table 3.5.: **Buffer A**

Tris-H_2SO_4 pH 9.4	0.1 M

Table 3.6.: **Buffer B**

D-Sorbit	1.2 M
KH_2PO_4 pH 7.4	20 mM

Table 3.7.: **Buffer C**

D-Sorbit	0.6 M
MES-Tris pH 6	5 mM
KCl	1 mM
EDTA	0.5 mM

Table 3.8.: **Protase inhibitor mixture** ($10,000\times$ stock)

Pepstatin	1 mg mL^{-1}
Antipain	2 mg mL^{-1}
Leupeptin	20 mg mL^{-1}

3.2.4. GAPDH activity assay

With the thawed cytosolic fractions an exchange of buffer C to the appropriate TEA (trieathanolamin, table 3.9) buffer was performed by an Econo-Pac 10DG Column (732-2010, Bio-Rad) according to its instruction manual. The collected fractions 2 and 3, each with a volume of 1 ml, were pooled and the total protein concentration was determined by Bio-Rad Protein Assay, based on the method of Bradford following the microtiter plate protocol (standard procedure). Bovine serum albumin (BSA) was used as a standard. After mixing the dye reagent with each sample (triplicates) the absorbances were measured immediately and after incubation of 5 minutes at 595 nm with a microplate reader (Spectrostar Nano, BMG Labtech).

Table 3.9.: **TEA buffer** pH 9.2

Triethanolamin	350 mM
Na_3PO_4	30 mM
ddH_2O	rest

Another method for buffer exchange was performed by Amicon Ultra 4 mL Centrifugal Filters 30KDa (Merck). After 4 mL cytosolic fraction were added to the centrifugal filters the centrifugation step was performed for 30 minutes at $4,000$ g and $4\,^{\circ}C$. The flow through was discarded and 3 mL TEA buffer added to the concentrated cytosol and centrifuged again. This step was repeated twice to get rid of the remaining buffer C. Next, the protein concentration of the buffer exchanged cytosol was measured by Bio-Rad Protein Assay, as described above.

The actual activity assay was performed according to Verho et al., 2002. The blank

componononents used for the *in vitro* assay (200 μM NAD(P)$^+$, 350 mM TEA buffer, $10 - 100$ μL cytosol) were mixed and measured over 5 minutes at 340 nm to determine possible variances of absorbances. After starting the reaction with 1 mM dihydroxyacetone phosphate (DHAP) the absorbance was observed over 10 minutes and the change per minute (ΔE min^{-1}) was obtained. The measured ΔE min^{-1} were normalized to the respective determined protein concentrations. The activity was calculated following the Beer-Lambert law (extinction coefficient of NAD(P)H: 6,200 L mol $^{-1}$ cm $^{-1}$). All measurements were performed as triplicates and carried out in 1 cm light path UV-Vis plastic cuvettes at room temperature.

3.2.5. Western blot

To prepare a crude protein extract 3 units OD600 of the desired strain were harvested (3,500 rpm, 5 minutes) at the indicated time points. The cells were disrupted according to Riezman (modification of Volland, 1993). Pellets were resuspended in 250 μL 1.85 M NaOH and 7.5% β-mercaptoethanol and incubated for 10 minutes on ice. 250 μL of 50% trichloroacetic acid (TCA) was added and incubated for one hour on ice. The precipitated protein was pelleted (13,000 rpm, 15 minutes, 4 °C) and washed with ice-cold deionized water. The supernatant was removed and the pellet resuspended in 50 μL 1xSDS-PAGE sample buffer and incubated at 95 °C for 10 minutes. The denatured samples were pelleted again and 15 μlL of the supernatant was loaded on the gel.

Sample separation was performed by SDS-PAGE (sodium dodecyl sulfate polyacrylamid gel electrophorese) for one hour at $30 - 40$ mA/gel using a 10% SDS gel. Color Protein Standard (Broad Range 11-245 kD, New England Biolabs) was used as a molecular weight standard. For the transfer to the nitrocellulose membrane 150 mA were applied to the transfer cassette for 75 minutes. Thereafter the membrane was blocked overnight at 4 °C with 5% milk powder in 1xTTBS (Tris-Tween-Buffer-Saline, table 3.10). On the next day, the membrane was washed once with 1xTTBS for 10 minutes and subsequently incubated with the corresponding primary antibody (anti-GFP: 1:1000 in 2.5% milk powder, anti-His6: 1:2000 in 2.5% milk powder) for one hour at room temperature. The membranes were washed 3 times for 10 minutes with 1xTTBS followed by the incubation with the second antibody (anti-mouse/anti-rabbit: 1:7500 in 2.5% milk powder). After another washing step with 1xTTBS the membrane was moistened with 2 mL of a chemiluminescence substrate (Thermo Scientific, luminol enhancer:peroxide solution 1:1), which enables the detection of the bound antibodies by ChemiDoc Imaging System (Bio-Rad).

Table 3.10.: **TTBS buffer**

Tris	50 mM
Tween 20	0.1%
NaCl pH 8.0	150 mM
ddH_2O	rest

3.2.6. Glycogen analysis

1×10^9 cells were harvested (centrifugation at 4,000 rpm for 5 minutes at 4 °C), washed with 4 °C cold distilled water and stored at −75 °C. 125 μL Na_2CO_3 were added to the cell pellets and incubated for 5 hours at 95 °C with shaking at 750 rpm. After spinning the samples they were put on ice for 5 minutes. The following steps were performed at room temperature. 75 μL of 1 M acetic acid and 300 μL of 0.2 M sodium acetate were added. D-glucose was released from glycogen by incubating the cells with 1.2 U mL^{-1} amyloglucosidase (58 U mg^{-1}, Sigma) overnight in a thermomixer (shaking $700 - 800$ rpm) at 57 °C. The overnight samples were put on ice and centrifuged at $16,000$ g for 30 seconds. The resulting glucose was determined with D-glucose-HK kit (Megazyme, Wicklow, Ireland) according to the manual. Measurements were performed as triplicates at 340 nm in 1 cm light path plastic cuvettes at room temperature.

3.2.7. Microscopy

Confocal fluorescence microscopy was performed with a Leica SP5 confocal microscope (Leica Microsystems, Mannheim, Germany) with spectral detection and a Carl Zeiss LSM510 (Carl Zeiss, Jena, Germany) with photomultiplier tubes (Hamamatsu Photonics, Hamamatsu City, Japan). Sample preparation and microscopic settings for visualization of GFP-tagged constructs were done as explained by Wolinski and Kohlwein, 2015.

4. Results

The aim of this thesis was to redirect the incorporated carbon sources towards TAG synthesis. To analyze the impact of the performed genetic mutations, the physiology of the strains listed in table 4.1 was characterized regarding their growth rates, their corresponding specific metabolite excretion rates and their specific glucose uptake rates (table 4.2).

Table 4.1.: Yeast strains used in this thesis

	Genotype	**Source**
CEN.PK 113-7D (wild type)	*Mat a URA3 TRP1 LEU2 HIS3*	P. Koetter
klaGAPDH	CEN.PK 113-7D *tdh3::GDP1opt-CYC1ter*	This thesis
klaGAPDH UTR1	CEN.PK 113-7D *tdh3::GDP1opt-CYC1ter* *tdh2::URA3-HXT7pro-UTR1opt*	This thesis
***klaGAPDH UTR1 adh1*Δ**	CEN.PK 113-7D *tdh3::GDP1opt-CYC1ter* *tdh2::URA3-HXT7pro-UTR1opt adh1*Δ	This thesis
HXT1	CEN.PK 113-7D *hxt1::PGK1pro-HXT1mut*	Klaus Natter

4.1. Physiology and growth

The characterization of each strain was carried out in minimal medium aerobic batch cultures with 20 g L^{-1} glucose (C-lim). The calculations of the specific uptake and excretion rates were done as described by Christen and Sauer, 2011 and the growth rates were obtained as stated in section 3.2.1. The measurements were performed with two independent biological replicates, except those of the *klaGAPDH* and *HXT1* mutants, which were performed once.

The *klaGAPDH UTR1* mutant showed a growth rate of 0.34 h^{-1}. The glucose uptake rate and the excretion rates could not be determined, as the measurements were executed at the very beginning of the exponential phase, hence, the concentrations of the glucose consumed or excreted metabolites were still too low to be detected by HPLC.

The growth rates of the *klaGAPDH* and *HXT1* mutants (0.36 h^{-1}, 0.38 h^{-1}) showed almost no difference to the wild type growth rate (0.41 h^{-1}). The *klaGAPDH UTR1 adh1*Δ mutant, in contrast, appeared to have a severe growth defect (0.18 h^{-1}), which also led to a lower glucose uptake rate (8.1 mmol g^{-1} h^{-1}) in comparison to the wild type (14.2 mmol g^{-1} h^{-1}). As the ORF of the *ADH1* was disrupted, the ethanol excretion rate was very low ($\approx 10\%$ of the wild type), whereas the glycerol excretion rate increased 3-fold (table 4.2). Table 4.3 shows the ethanol and glycerol excretion per consumed glucose of the *klaGAPDH* and *klaGAPDH UTR1 adh1*Δ mutant in comparison to the wild type. The *klaGAPDH* mutant excreted lower ethanol amounts than wild type. This effect is most likely due to a lower cytosolic NADH concentration, hence, less NADH has to be oxidized via ethanol production. The excreted glycerol amounts showed a doubling and even a 7-fold increase of the *klaGAPDH* and *klaGAPDH UTR1 adh1*Δ mutant, respectively, in comparison to the wild type.

The biomass yields per consumed glucose were measured in the beginning of stationary phase, when all the glucose was consumed. The results range between 0.07 and 0.21 $g_{biomass}$ $g^{-1}_{glucose}$ (table 4.2). The former represents the yield of the mutant *klaGAPDH UTR1 adh1*Δ, which is very low, most likely caused by the high amounts of excreted glycerol (5.7 ± 1.3 mmol g^{-1} h^{-1}). Additionally, the biomass formation of the *klaGAPDH UTR1 adh1*Δ mutant already stops around 5×10^9 biovolume fL mL^{-1} in C-lim. Wild type cells as well as the other mutant strains stop growing at ca. 1×10^{10} biovolume fL mL^{-1}.

Table 4.2.: **Growth parameters in C-lim**: *klaGAPDH UTR1* mutant is not stated, see text for details.

	wild type	***klaGAPDH***	***klaGAPDH UTR1 adh1*Δ**	***HXT1***
Growth rate (h^{-1})	0.41 ± 0.02	0.36	0.18 ± 0.01	0.38
Glucose uptake (mmol g^{-1} h^{-1})	14.23 ± 0.04	11.2	8.1 ± 0.2	13.2
Glycerol excretion (mmol g^{-1} h^{-1})	1.59 ± 0.03	2.2	5.7 ± 1.3	1.7
Acetate excretion (mmol g^{-1} h^{-1})	0.37 ± 0.04	0.23	0.30 ± 0.09	0.38
Ethanol excretion (mmol g^{-1} h^{-1})	20.2 ± 0.1	14.8	2.2 ± 0.3	21.0
Biomass yield ($g_{biomass}$ $g^{-1}_{glucose}$)	0.209 ± 0.006	0.180 ± 0.014	0.069 ± 0.006	$0,221 \pm 0,002$

Table 4.3.: **Ethanol and glycerol excretion per consumed glucose [mmol mmol^{-1}]** in C-lim batch cultures

	ethanol	**glycerol**
wild type	1.4	0.11
klaGAPDH	1.3	0.20
***klaGAPDH UTR1 adh1*Δ**	0.3	0.70

4.2. Redox-reprogrammed mutants

The results of the *klaGAPDH*, *klaGAPDH UTR1* and the *klaGAPDH UTR1 adh1*Δ mutants are presented separately from the *HXT1* mutant, to which chapter 4.3 is dedicated.

4.2.1. Lipid contents

Besides the physiological parameters stated in table 4.2, the lipid content of the strains was investigated. Therefore the cells were cultivated in C-lim and harvested during exponential growth and in stationary phase. The lipid extraction and analysis were performed as described in chapter 3.2.2. Three lipid species (TAG, ERG and sterol ester (SE)) were measured by thin layer chromatography (TLC). Each measurement was carried out twice to consider the technical variance. Additionally, at least three independent biological replicates were examined.

The exponentially growing strains showed no significant differences. The wild type TAG content was found to be 1.1% of biomass. A slight increase of TAG was observed for the *klaGAPDH*, *klaGAPDH UTR1* and klaGAPDH UTR1 adh1Δ mutants (1.3%, 1.6% and 1.5% of biomass respectively). In stationary phase the TAG content of the wild type was similar to exponential phase. The *klaGAPDH UTR1 adh1*Δ mutant showed increased values (1.8% of biomass), whereas the contents of the *klaGAPDH* and *klaGAPDH UTR1* mutants decreased (1.0% and 1.1% of biomass).

The second investigated lipid species ERG plays an important role in maintaining the fluidity of fungal cell membranes, comparable to the role of cholesterol in mammal cell membranes (Parks and Casey, 1995). In this case the ERG measurements serve as a control. The content should stay around 4 mg g^{-1} dry weight (DW) in all strains, which complies with the results of the analyzed strains (figure 4.2).

Sterol esters, on the other hand, represent another storage possibility for fatty acids in the cell (Parks and Casey, 1995, Yang et al., 1996). Therefore, increased SE values indicate a higher utilization of carbon resources for sterol synthesis, which may compete

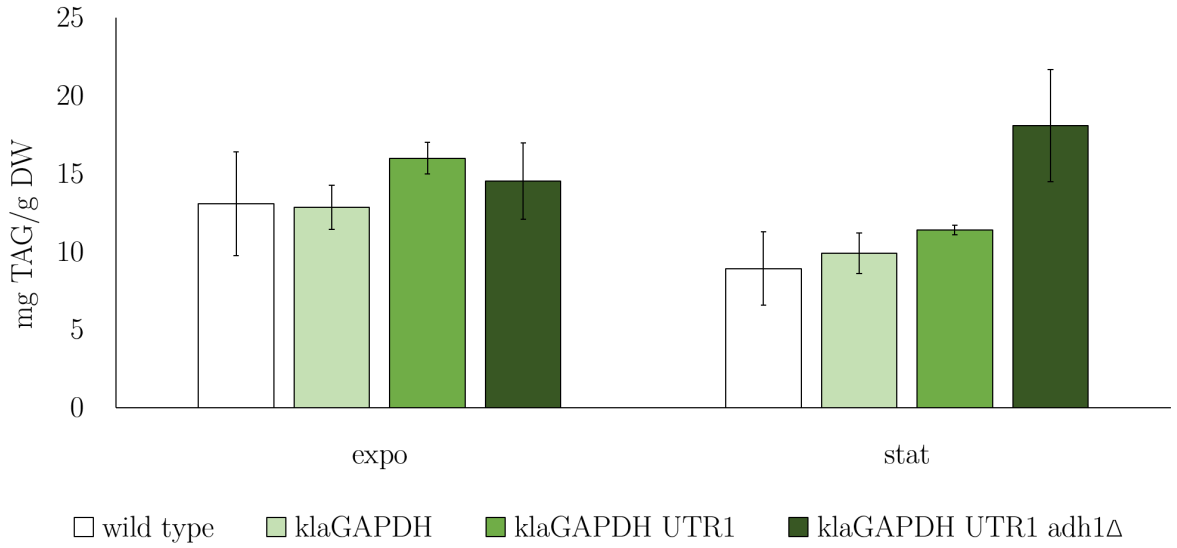

Figure 4.1.: **TAG content** in C-lim batch cultures, **expo** refers to exponential phase and **stat** to stationary phase.

with TAG synthesis. Only the *klaGAPDH UTR1 adh1*Δ mutant showed a 4-fold increase (1.2% of biomass) in stationary phase (figure 4.3).

The lipid content of nitrogen starved cells was also investigated. It is known that yeast cells start to accumulate lipid under nitrogen limited conditions (Kolouchová et al., 2016, Albers et al., 1996). Therefore, the cells were cultivated in N-lim batch cultures and harvested after 48, 72 and 96 hours for lipid analysis (see figure 4.4). The TAG content of the *klaGAPDH* mutant increased significantly compared to wild type (1.4-fold after 48 hours, 1.5-fold after 72 hours and 1.3-fold after 96 hours cultivation, p-values: $0.0022, 0.026, 0.004$), whereas the *klaGAPDH UTR1* mutant shows a tremendous drop in TAG content. This may be due to the severe growth defect the strain shows under nitrogen starved conditions. Its dry weight was measured to be 0.7 g L^{-1} after 72 hours of cultivation, whereas the wild type showed a dry weight of 1.5 g L^{-1} (table 4.4). The *klaGAPDH UTR1 adh1*Δ mutant showed a stepwise increase of the TAG content ranging from 5.1 to 9.1% and finally after 96 hours even 10.1% of biomass. Nevertheless, the dry weight of 0.8 g L^{-1} remained very low (table 4.4). The *klaGAPDH* mutant showed a slight increase of ERG (figure 4.5), which is most likely due to the higher concentration of the cytosolic NADPH caused by klaGAPDH. ERG synthesis requires NADPH as well (Parks and Casey, 1995). An enhanced ERG synthesis also leads to higher amounts of SE, which was observed for the *klaGAPDH* mutant (1.4-fold, figure 4.6).

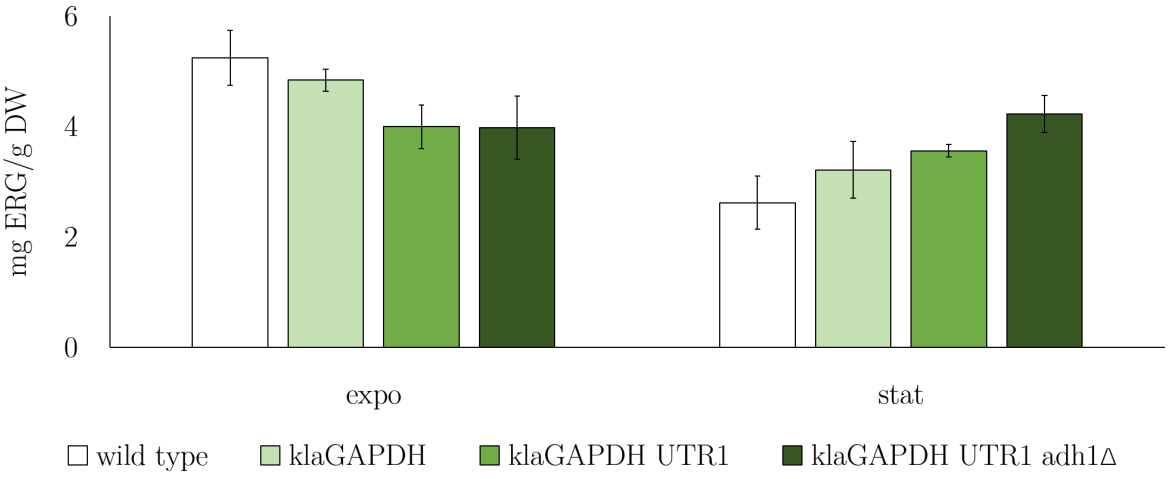

Figure 4.2.: **ERG content** in C-lim batch cultures.

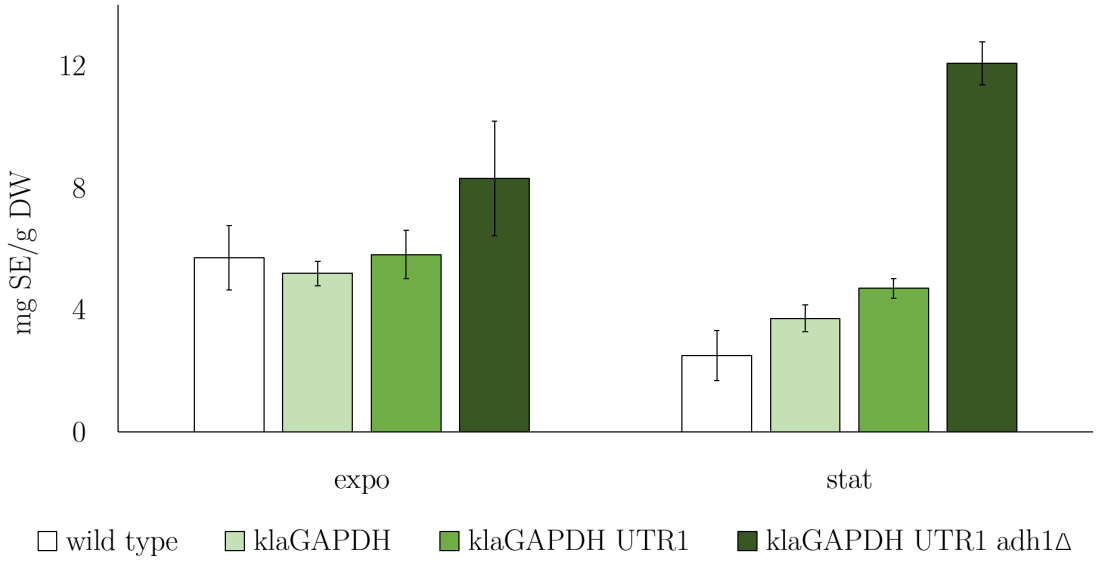

Figure 4.3.: **SE content** in C-lim batch cultures.

Table 4.4.: **Dry weights** after 72 hours cultivation of nitrogen starvation

wild type	1.5 ± 0.2 g L^{-1}
klaGAPDH	1.4 ± 0.2 g L^{-1}
klaGAPDH UTR1	0.7 ± 0.1 g L^{-1}
klaGAPDH UTR1 adh1Δ	0.8 ± 0.1 g L^{-1}

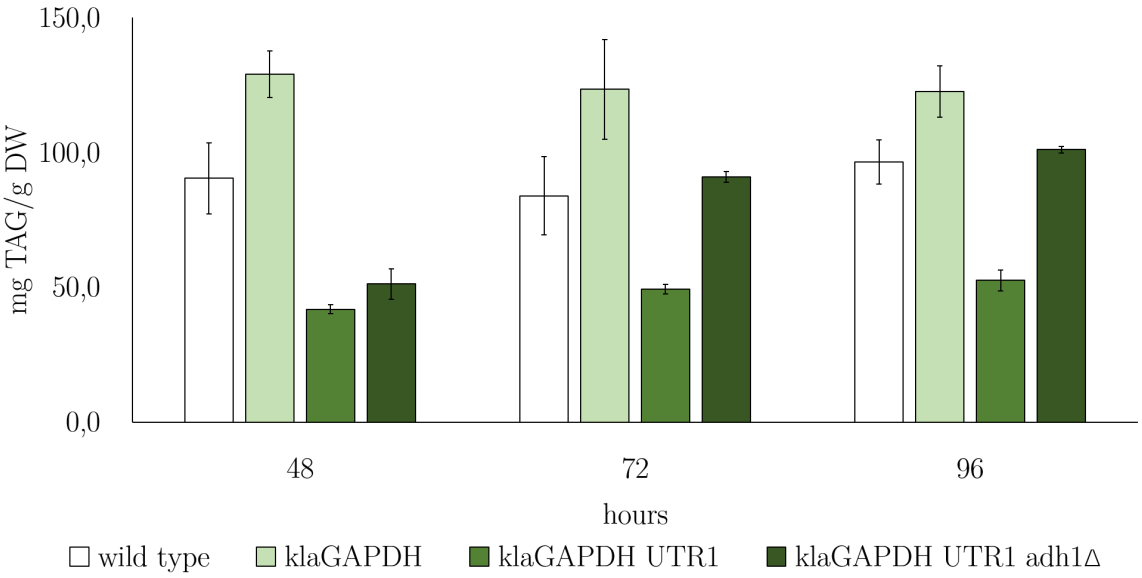

Figure 4.4.: **TAG content** in N-lim batch cultures.

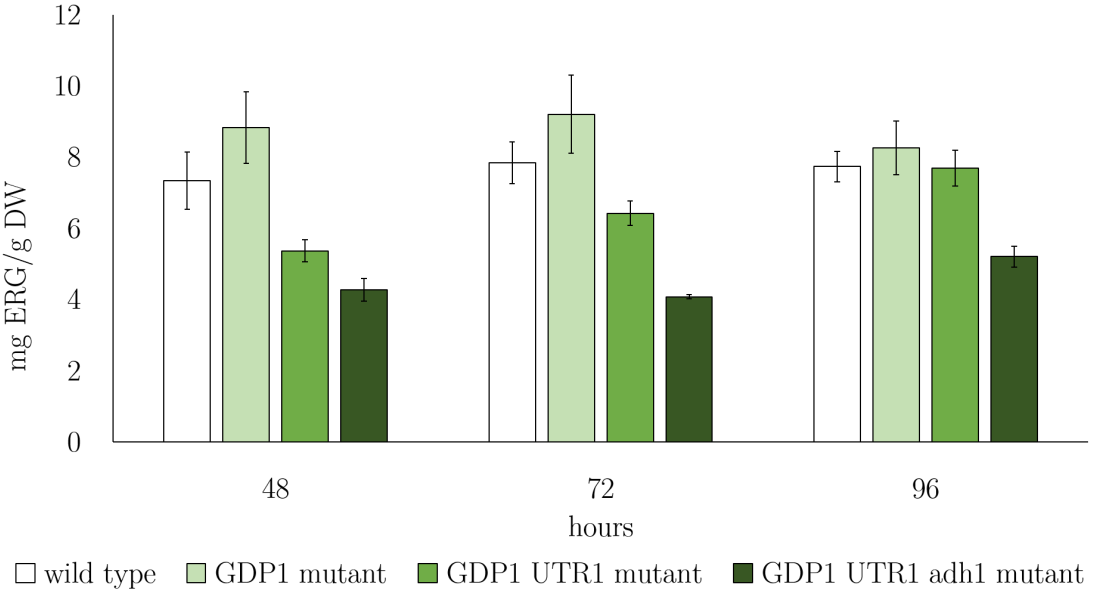

Figure 4.5.: **ERG content** in N-lim batch cultures.

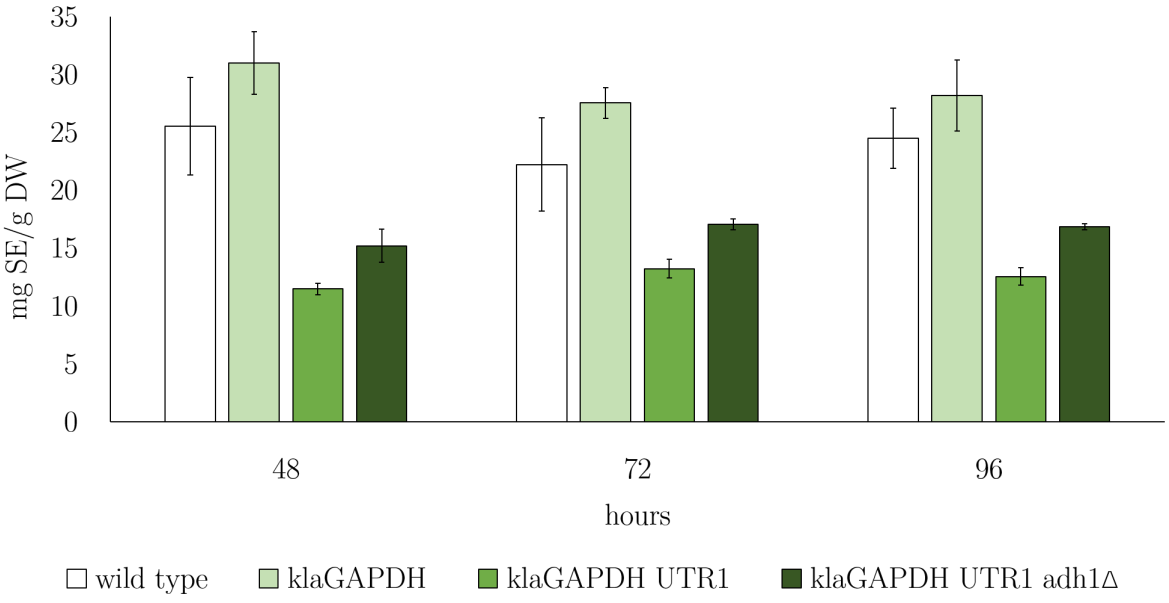

Figure 4.6.: **SE content** in N-lim batch cultures.

4.2.2. Glucose uptake and glycerol excretion of nitrogen starved cells

To better understand the metabolism of the mutants and to determine possible differences, the excreted metabolites and consumed glucose of nitrogen starved cells were investigated. The samples were measured by HPLC. The obtained concentrations were normalized to the respective dry weights of the strains. Each measurement was performed with three independent biological replicates.

The glucose consumption of N-lim batch cultures seemed to increase with each genetic intervention, led by the wild type showing the lowest incorporation and followed by *klaGAPDH*, *klaGAPDH UTR1* and *klaGAPDH UTR1 adh1*Δ with the highest uptake per gram dry weight (figure 4.7). This leads to the assumption that the engineered strains, especially *klaGAPDH UTR1* and *klaGAPDH UTR1 adh1*Δ, are counterbalancing a metabolic defect by incorporating a higher amount of energy (in the form of glucose). Table 4.8 shows the glucose concentrations (g L^{-1}) left in the medium after 48, 72 and 96 hours of cultivation. Only the *klaGAPDH* mutant consumed the 20 g glucose in the medium. The wild type, the *klaGAPDH UTR1 adh1*Δ mutant as well as the *klaGAPDH UTR1* mutant still had glucose left in the medium after 96 hours of cultivation (5 g L^{-1} and 9 g L^{-1}).

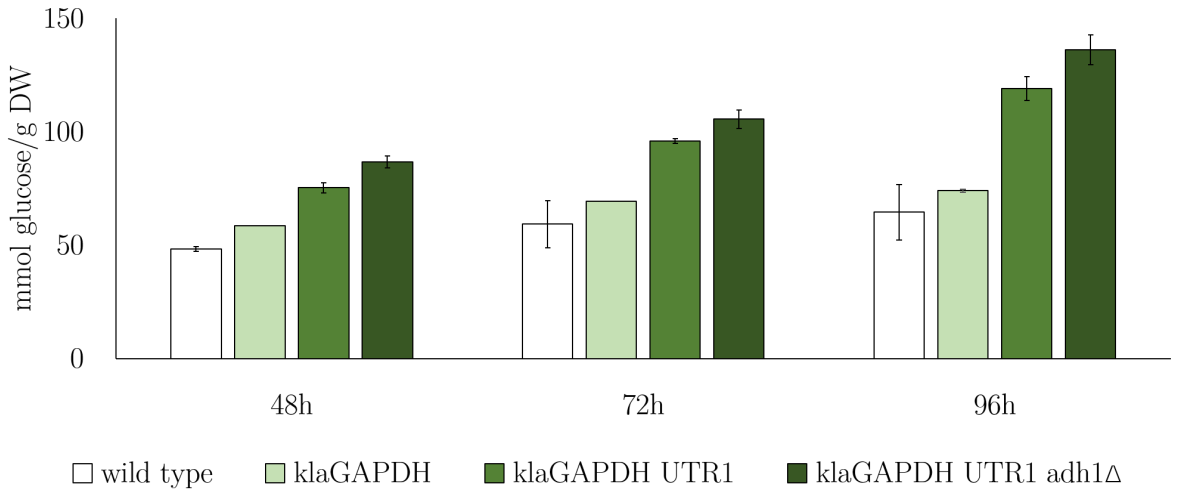

Figure 4.7.: **Glucose uptake** in N-lim batch cultures.

The most important differences were observed regarding glycerol excretion. Glycerol is

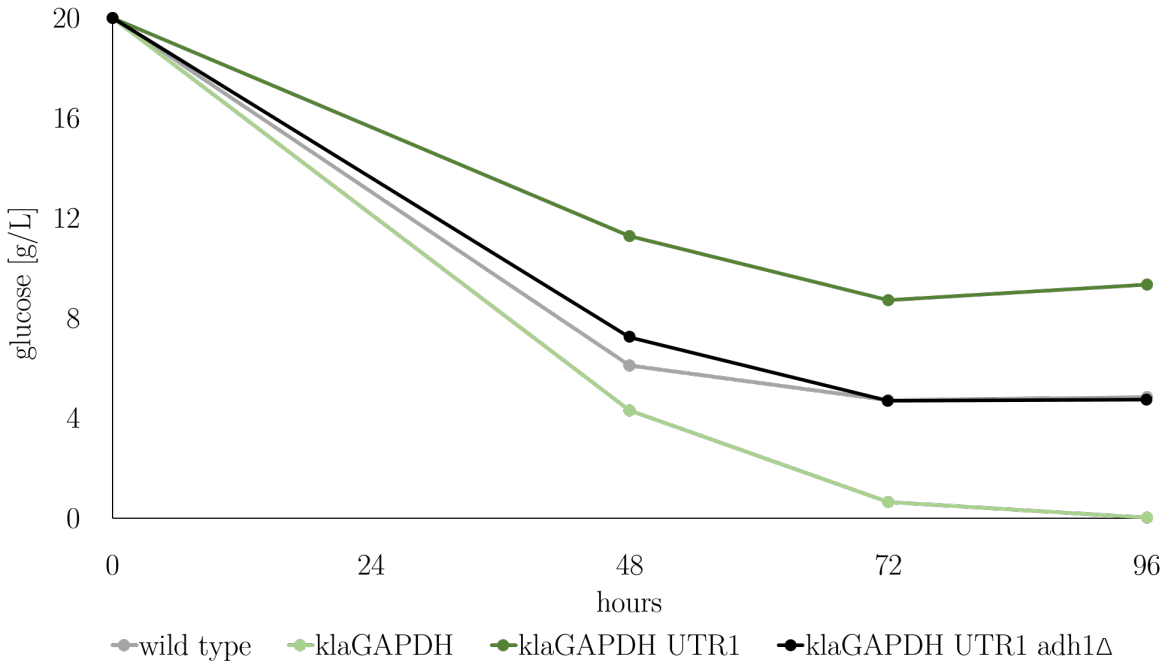

Figure 4.8.: **Absolute glucose consumption** in N-lim batch cultures.

synthesized from DHAP to glycerol-3-phosphate catalyzed by glycerole-3-phosphate dehydrogenase (G3PD) and further dephosphorylated by glycerole-3-phosphatase (G3Pase) to glycerol. Therefore, some of the glycolytic carbon source is used for glycerol synthesis. The main reason for this is the reoxidation of the produced cytosolic NADH. This provides the ability to maintain the cellular redox balance. As a consequence this carbon source is missing for pyruvate formation, which also might affect fatty acid synthesis.

As shown in figure 4.9 the glycerol excretion of the *klaGAPDH UTR1 adh1*Δ mutant was highly increased, as already observed in exponentially grown cells (table 4.2 and 4.3). To a lesser extent this was also observed for the *klaGAPDH UTR1* mutant and the *klaGAPDH* mutant. Similar to the glucose consumption also the glycerol excretion increased with every metabolic intervention. This leads to the assumption, that at least one part of the additionally incorporated glucose gets metabolized to glycerol.

Ethanol exrection was not observed for nitrogen limited batch cultures, as most of the ethanol evaporates during such a long cultivation time. Therefore, the results are not representative. However, ethanol values of exponentially grown cells were compared (table 4.2). Data about acetate excretion are not presented, as the measurements show very high variation coefficients ($\geq 50\%$).

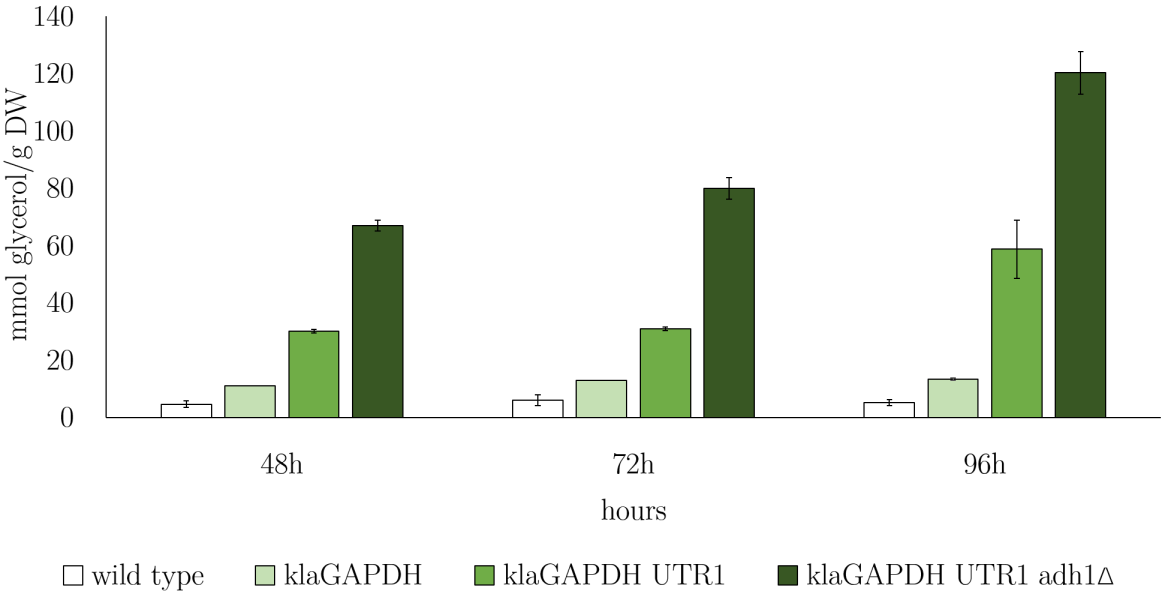

Figure 4.9.: **Glycerol excretion** in N-lim batch cultures.

4.2.3. klaGAPDH and NAD(H)-kinase expression

Next, the expression of the integrated Proteins klaGAPDH and NAD(H)-kinase was investigated. The samples were withdrawn from cultivations for lipid analysis. Therefore, each strain was tested in exponential growth and stationary phase (C-lim batch cultures, figure 4.10) as well as under nitrogen starved conditions after 48, 72 and 96 hours of cultivation (figure 4.11). The western blots were performed as described in section 3.2.5.

The codon optimized and HIS-tagged klaGAPDH has a molecular weight of 39.9 kilo Dalton (kD) and was highly expressed even in stationary phase and under nitrogen starved conditions in all three strains (*klaGAPDH*, *klaGAPDH UTR1* and *klaGAPDH UTR1 adh1*Δ). The codon optimized and HIS-tagged NAD(H)-kinase in contrast showed almost no expression in the respective UTR1 mutants, not even in exponential phase.

Surveying the *klaGAPDH UTR1* mutant, a slight band at the height of 60 kD after 48 hours was noticeable, which most likely represents the NAD(H)-kinase. The band disappeared after 72 and 96 hours. Hence, the protein might not be stable. However, the *klaGAPDH UTR1 adh1*Δ mutant showed a different result. The NAD(H)-kinase seemed to be still expressed after 96 hours of nitrogen starvation. Additionally, a slight band was visible in the upper part at $\approx$ 80 kD. This might be a dimeric formation of the overexpressed klaGAPDH.

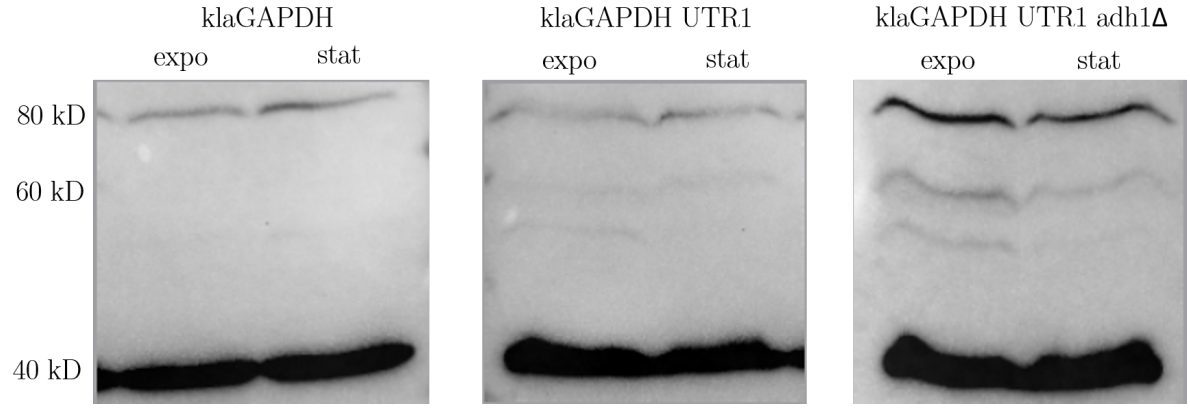

Figure 4.10.: **Western blot**: C-lim batch cultures.

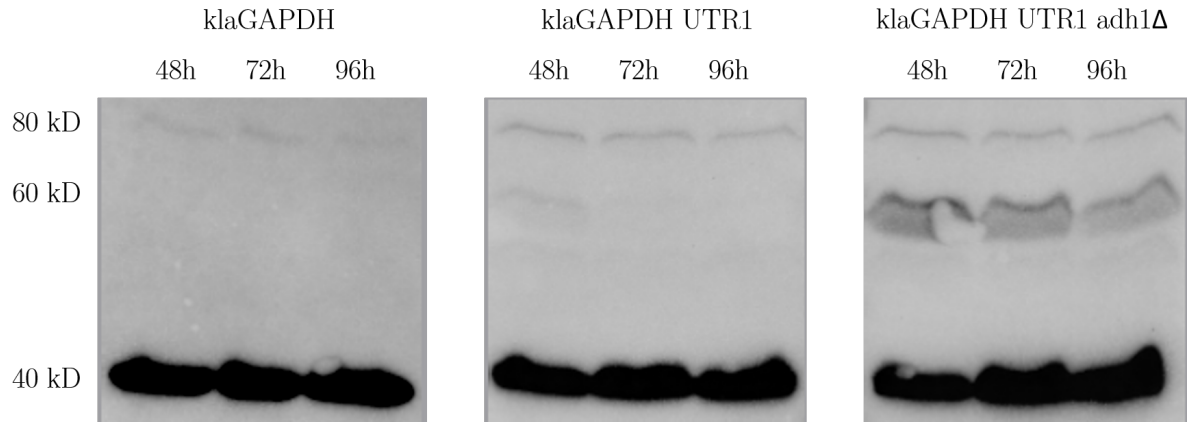

Figure 4.11.: **Western blot**: N-lim batch cultures.

4.2.4. klaGAPDH activity

Furthermore the activity of the integrated klaGAPDH was investigated by a kinetic assay following Verho et al., 2002. C-lim batch cultures were harvested in late exponential phase ($5 - 8 \times 10^7$ cells mL^{-1}). The purification of the cytosolic fraction was performed as stated in section 3.2.3 and stored at $-20\,°C$ until the assay was carried out. After thawing on ice the buffer of the fractions was exchanged. Next, the total protein concentration of each sample was determined by *Bradford* protein assay (see 3.2.4). The activity assay was done with two different cofactors NAD^+ and $NADP^+$ and each sample was measured three times. The results were normalized based on the examined protein concentrations (see figure 4.12).

As already mentioned in the introduction, the klaGAPDH was reported to have similar affinities for both of the used cofactors, which was confirmed by this assay. The substrate, which was used to start the assay was DHAP. DHAP does not directly represent the

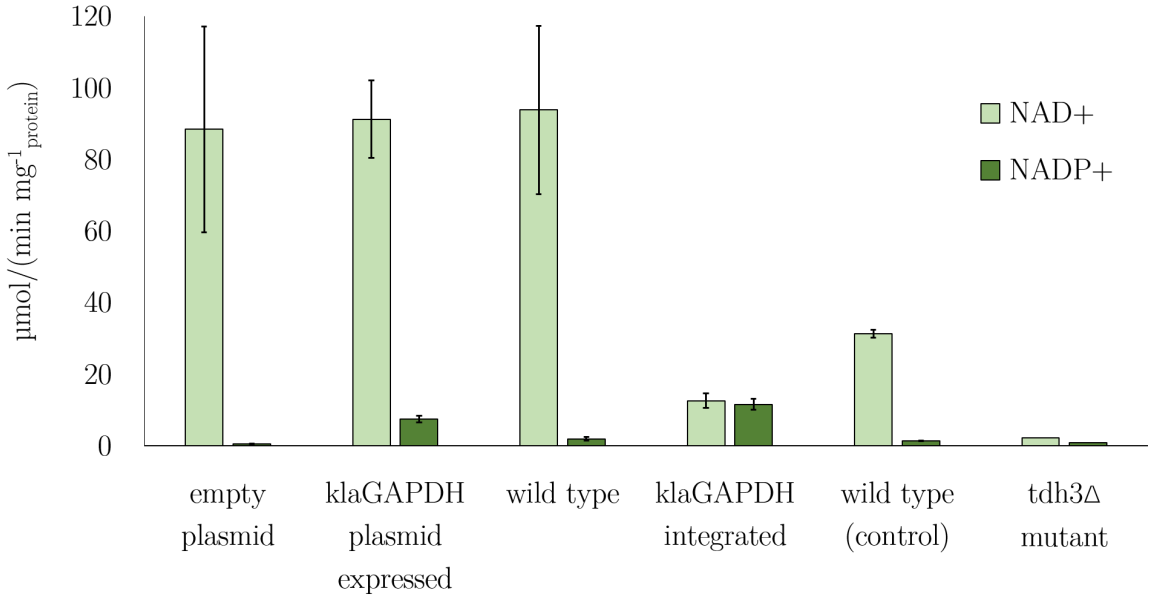

Figure 4.12.: **Activity assay** of klaGAPDH with NAD^+ and $NADP^+$ as cofactors.

substrate of GAPDH, first it has to be converted to GAP by the triose phosphate isomerase (TPI). The equilibrium of this reaction is strongly on the side of DHAP (Rozovsky and McDermott, 2007, Harris et al., 1998), which means that the consumption of GAP by klaGAPDH results in a change of the GAP concentration. Changing the conditions of the previously adjusted steady state by TPI triggers the reaction rate, as the system attempts to oppose the change (Le Chatelier's principle). In other words, the activity of klaGAPDH relies on DHAP conversion to GAP. This *in vivo* like situation is only possible as the cytosolic fraction contains all cytosolic proteins, hence, also TPI. Moreover, TPI is known as the "catalytically perfect enzyme" as described by Albery and Knowles, 1976. The reaction rate of TPI is only limited by the diffusion of substrate and product (Rose, Fung, and Warms, 1990). Using DHAP as the substrate, therefore, does not influence the activity of klaGAPDH. This was confirmed by performing the assay with GAP as a substrate. The only difference was the necessity of additional time, as the system first had to achieve equilibrium by TPI conversion. Then the reaction was started by adding the respective cofactor, instead of adding the substrate.

First, the GAPDH assay was performed with strains carrying an empty vector or a plasmid expressing *klaGAPDH*. Using NAD^+ as a cofactor, the obtained activity was 91 ± 11 and 88 ± 29 μmol min^{-1} mg^{-1} protein, for the expression strain and the control, respectively. The $NADP^+$ dependent activity of klaGAPDH increased 9−fold in comparison to the control strain (figure 4.12).

The activity of the *klaGAPDH* mutant showed similar results with both cofactors. The total activity (NAD^+- and $NADP^+$-activity) was observed as 24 μmol min^{-1} mg^{-1} protein, which represents only 25% of the wild type activity (96 μmol min^{-1} mg^{-1} protein).

To confirm that the observed activity of the *klaGAPDH* mutant derived from the integrated klaGAPDH, the assay was repeated with a tdh3Δ strain (section 3.1.2). The two remaining native GAPDH encoding genes *TDH2* and *TDH1* might have contributed to the prior determined klaGAPDH activity. Surprisingly, only a very low activity was observed using both cofactors, namely 2.3 with NAD^+ and 0.9 μmol min^{-1} mg^{-1} with $NADP^+$. The control strain (wild type) showed an activity of 31 μmol min^{-1} mg^{-1}, which did not match with the wild type activity of prior measurements 4.12.

4.3. *HXT1* mutant

The *HXT1* mutant was designed to prevent ubiquitination followed by degradation of Hxt1p under nitrogen limited conditions. GFP-tagging of *HXT1mut* and *HXT1wt* allowed to directly observe differences of degradation under the microscope (see section 3.2.7). The respective GFP-tagged strains (*HXT1* mutant and CEN.PK113-7D) were cultivated in C-lim and N-lim batch cultures.

The exponentially grown cells showed differences regarding the signal intensity most likely caused by the overexpression of *HXT1mut*. Moreover, *HXT1mut* localized to the cell membrane and the vacuole, whereas most of the wild type cells show either a signal in the membrane or in the vacuole (figure 4.13). In stationary phase the cells showed more obvious differences. In contrast to the *HXT1* mutant, no signal at all was observed in the wild type cell membrane. With this it was shown that degradation of Hxt1p in the mutant takes place, but not to such an extent as in the wild type (figure 4.14).

In nitrogen starved cells again a brighter signal was detected in mutant cells, especially in the vacuole after 48 hours of cultivation. Nevertheless, a weak signal was still observable in the cell membrane after 24 and 48 hours. In contrast, the wild type showed no signal at all, neither derived from its cell membrane nor from its vacuole (figures 4.15, 4.16). These observations confirm the effect of a stabilization of Hxt1p in the cell membrane, even though Hxt1p still gets degraded.

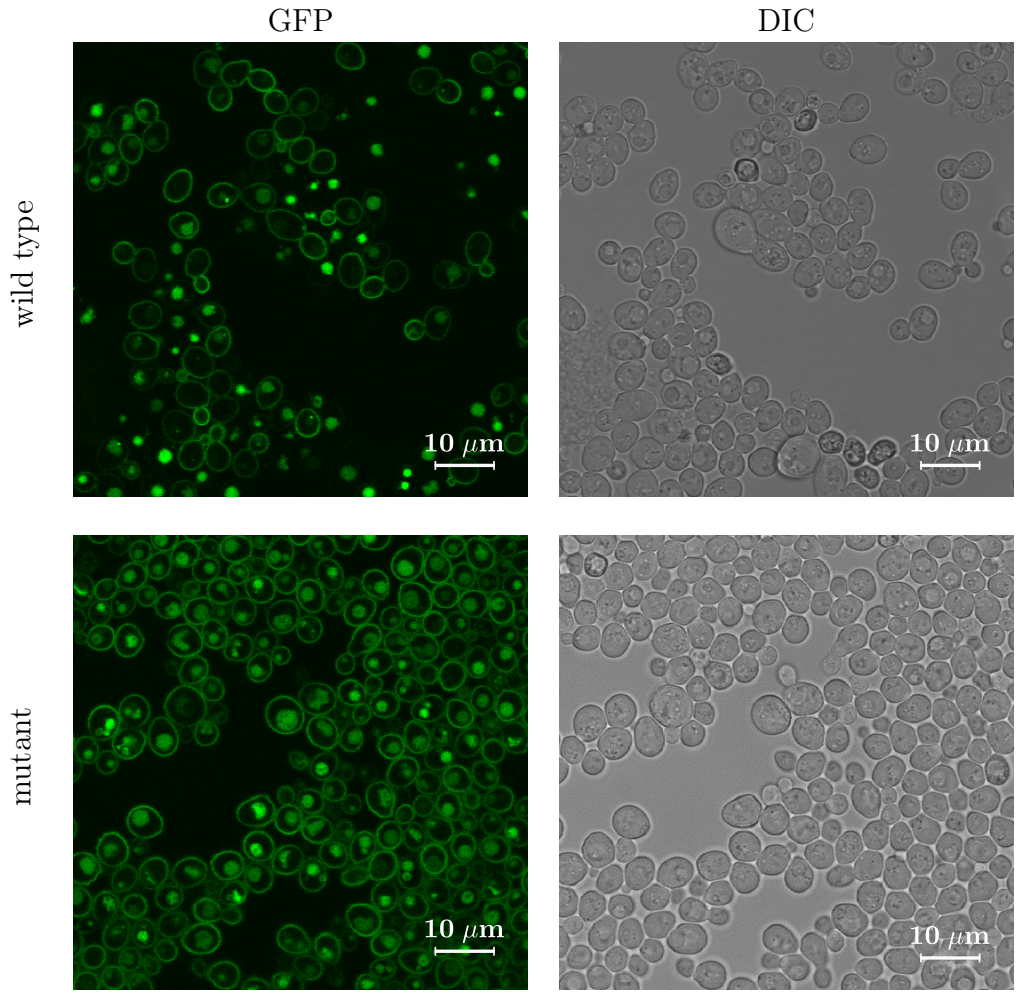

Figure 4.13.: Fluorescence microscopy of the mutant and wild type Hxt1p-GFP constructs: **exponential phase C-lim batch cultures, DIC** differential interference contrast.

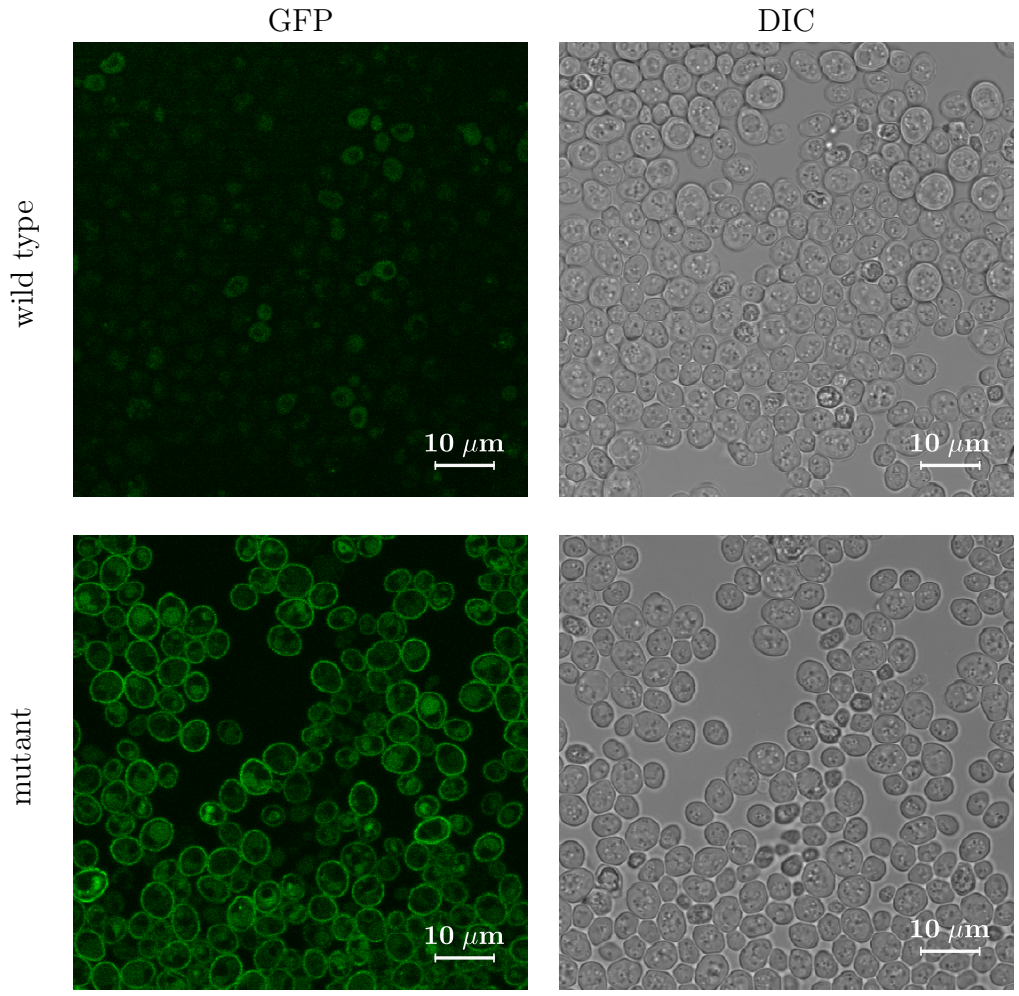

Figure 4.14.: Fluorescence microscopy of the mutant and wild type Hxt1p-GFP constructs: **stationary phase C-lim batch cultures**.

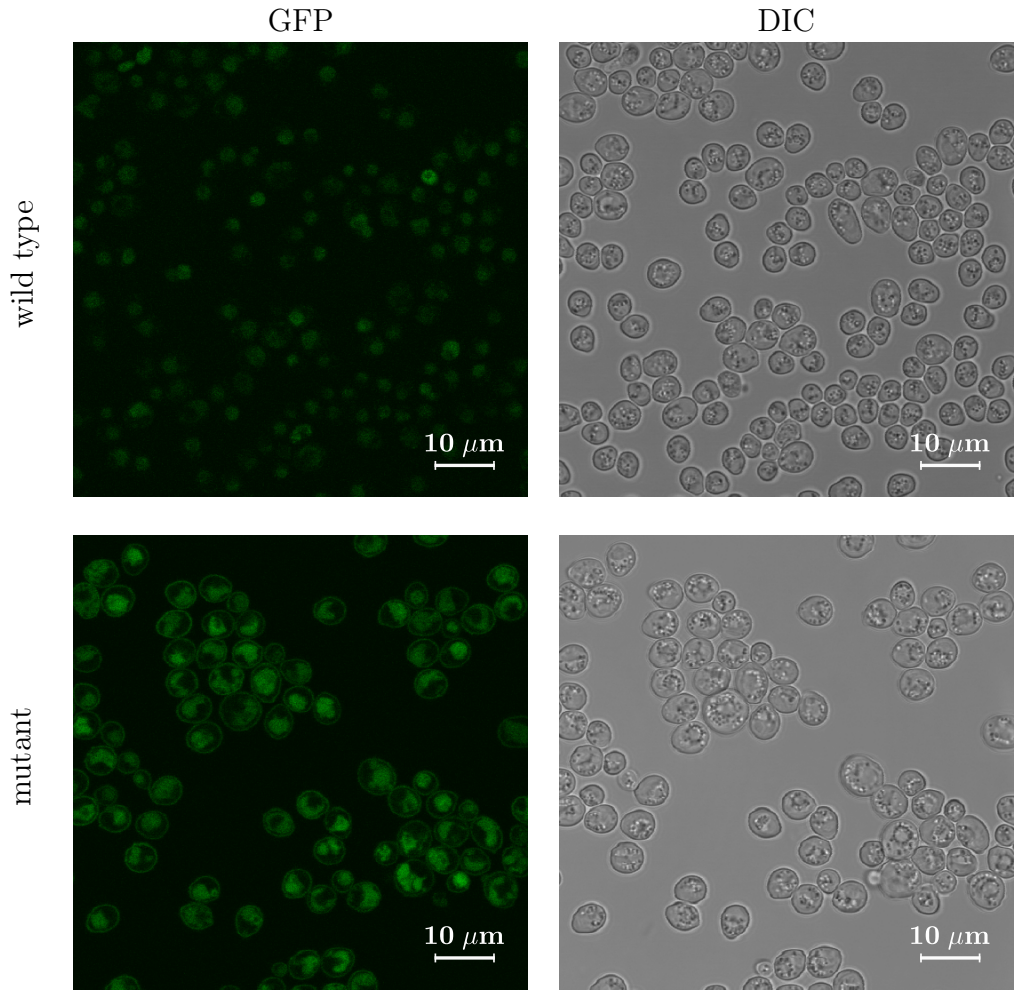

Figure 4.15.: Fluorescence microscopy of mutant and wild type Hxt1p-GFP constructs: **N-lim batch cultures after 24 hours of cultivation**.

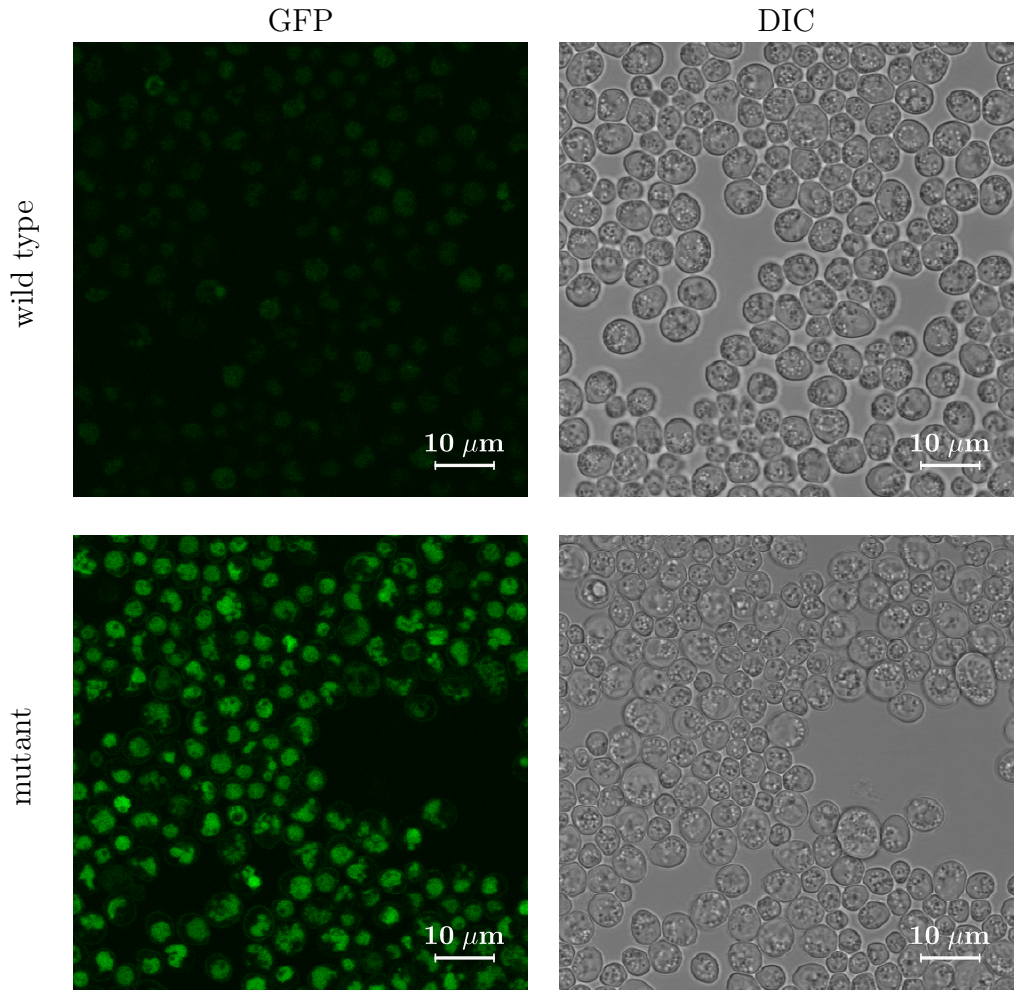

Figure 4.16.: Fluorescence microscopy of mutant and wild type Hxt1p-GFP constructs: **N-lim batch cultures after 48 hours of cultivation**.

Next, the expression levels of both Hxt1p-GFP constructs (89 kD) were investigated using identical cultivation conditions. Exponentially grown mutant cells showed a bright band at 90 kD, in contrast to the wild type. This difference can be assigned to the overexpression of the mutated Hxt1p. In stationary phase the wild type showed a band at 26 kD similar to the mutant, which represents the molecular weight of the non-fused form of GFP. Hence, this might be a degradation product of the Hxt1p-GFP construct. The mutant still showed expression of Hxt1p in stationary phase (figure 4.17a).

Nitrogen starved cells had similar expression levels as cells in stationary phase. Bright bands shown by mutant cells and faint bands shown by wild type cells at 26 kD were detected. Moreover, the mutant still expressed the entire Hxt1p-GFP construct. These signals were comparable to those determined by microscopy. The observed fluorescence

in the vacuole most likely derived from the degradation product (26 kD) and the signal obtained from the cell membrane might represent Hxt1p-GFP (89 kD).

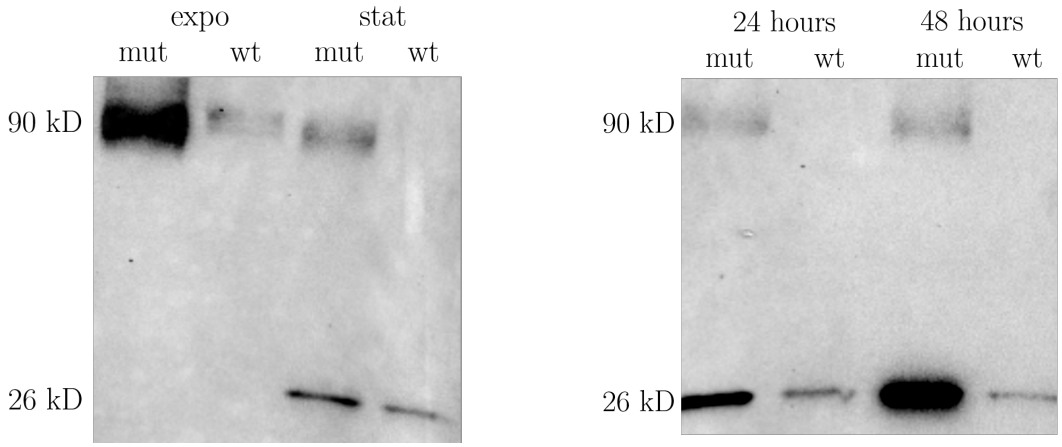

(a) C-lim (b) N-lim

Figure 4.17.: **Expression of the mutant and wild type Hxt1p-GFP constructs** under different conditions: **(a) expo**nential and **stat**ionary **C-lim** batch cultures, **(b) N-lim** batch cultures after **24 hours** and **48 hours** of cultivation.

Furthermore, the glucose uptake of the *HXT1* mutant was compared with wild type under nitrogen starved conditions. Therefore, culture medium was withdrawn and measured by HPLC in 12 hours intervals. As expected, the glucose uptake of the *HXT1* mutant was already increased after 12 hours of cultivation. After this time point, the glucose uptake in the wild type was almost completely arrested, although there was still glucose available (4-5 g L^{-1}). The mutant completely consumed all the glucose after 48 hours of cultivation (figure 4.18). Further measured metabolites in the medium (ethanol, acetate and glycerol) showed concentrations similar to the wild type.

In order to find out how the additional incorporated glucose of the *HXT1* mutant gets metabolized, the TAG and glycogen contents were analyzed. The TAG content of the two strains showed no differences (figure 4.19). In contrast, the glycogen content of the mutant was increased by 25%, as compared to the wild type (figure 4.20).

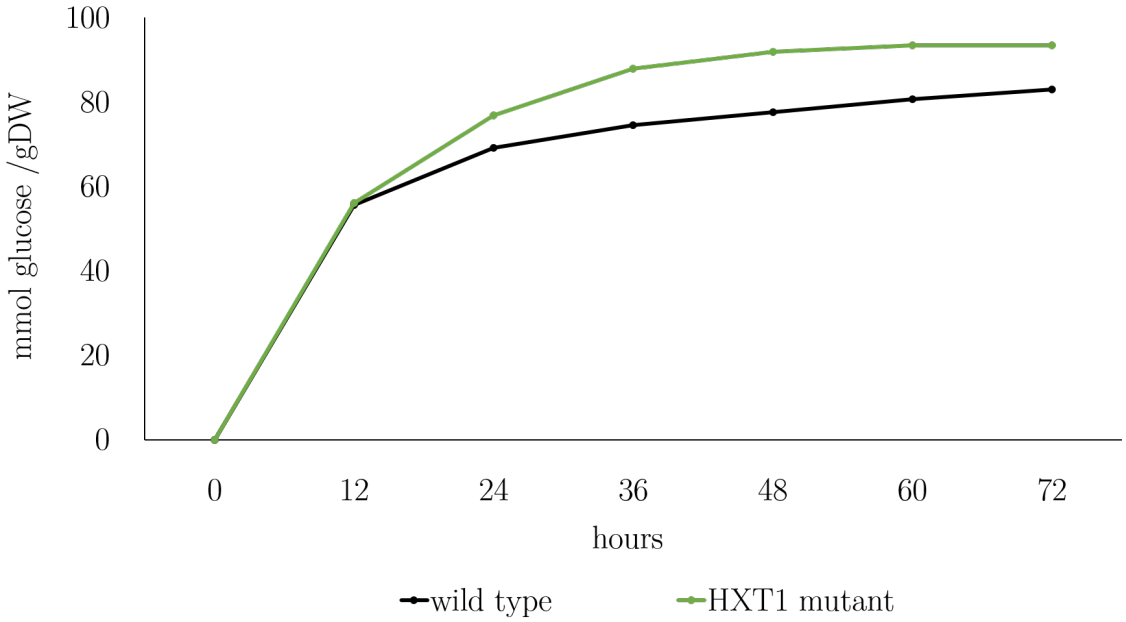

Figure 4.18.: **Glucose uptake in N-lim batch cutlures**: *HXT1* mutant vs. wild type.

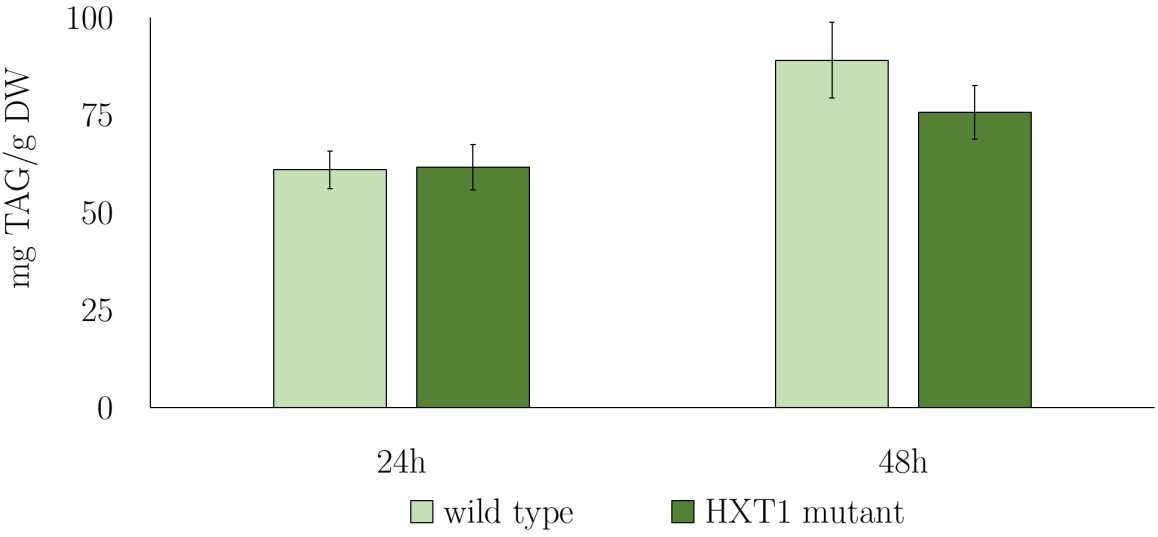

Figure 4.19.: **TAG content *HXT1* mutant vs. wild type**, N-lim batch cultures after 24 and 48 hours of cultivation.

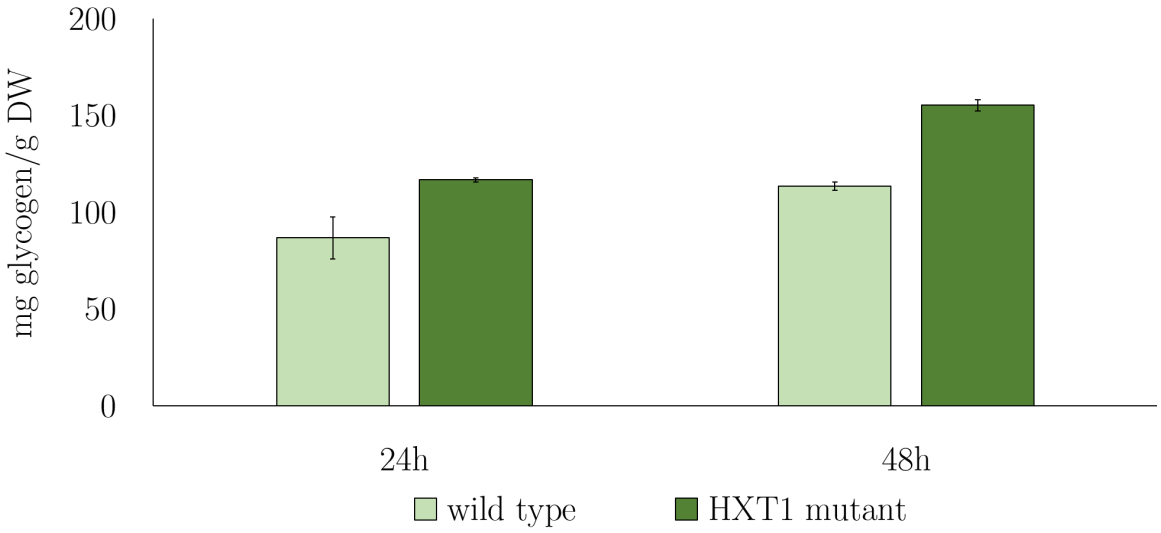

Figure 4.20.: **Glycogen content of *HXT1* mutant vs. wild type**, N-lim batch cultures after 24 and 48 hours of cultivation.

5. Discussion

5.1. *klaGAPDH* mutant

One of the first performed experiments was the activity assay. In the beginning a plasmid expressed klaGAPDH was tested, which showed a slight increase of the klaGAPDH activity using $NADP^+$ as a cofactor of 0.6 to 7.5 μmol min^{-1} mg^{-1} protein. The activity withNAD^+, in contrast, was much higher and comparable to the wild type activity, as the native GAPDH encoded by *TDH3* was still expressed.

The activity shown by the *klaGAPDH* mutant was very low. Due to the cloning strategy, klaGAPDH integration resulted in deletion of *TDH3*. *TDH3* represents the gene, which encodes the most active GAPDH (50 to 60% of the total activity) of all three *TDH* genes (McAlister and Holland, 1985). Therefore, the NAD^+ dependent activity decreased drastically (13.6% of the wild type activity), whereas the $NADP^+$ activity increased (6-fold). Nevertheless, it could not be excluded that the remaining NAD^+-activity was derived from the two other native GAPDH proteins, encoded by *TDH2* and *TDH1*. Therefore, *TDH3* of the wild type strain was deleted to test its activity.

The activity of the *tdh3*Δ mutant was almost not detectable (2.4% of the wild type), although it is known that the isozymes encoded by *TDH1* and *TDH2*, contribute $10-15\%$ and $25-30\%$ to the total GAPDH activity (McAlister and Holland, 1985). However, their expression levels also depend on environmental conditions, for instance *TDH1* is primarily expressed during stationary phase (Delgado et al., 2001). Regarding this result, the observed activity of the *klaGAPDH* strain might be completely derived from klaGAPDH, but this assumption leads to the question: How is the cell able to survive with such a low GAPDH activity? The only possibility is to drastically drive down the metabolism, which would result in a growth phenotype. The growth rate was determined as 0.37 h^{-1}, which is comparable to the wild type growth rate (0.4 h^{-1}). This observation indicates that the activity most likely got lost during cytosolic fractionation or buffer exchange. Even the wild type, which was treated equally, showed an activity loss of 66% in comparison to the obtained activity from prior measurements. Therefore, this activity loss must be caused by a methodological error. Instead of the usually used gel filtration, the buffer exchange was performed by Centrifugal Filter Units, which concentrate proteins with a molecular weight of at least 30 kD. Therefore, TPI most likely got lost, as it exhibits a molecular weight of 26.8 kD and a conversion of DHAP to

GAP was not possible anymore, which negatively affected the availability of GAP as a substrate for GAPDH. A buffer exchange using gel filtration was not repeated with the tdh3Δ mutant.

In general it was confirmed that klaGAPDH has similar affinity for both cofactors. Anyhow, the *klaGAPDH* mutant lost 75% of the wild types GAPDH activity. One possible explanation for this loss of activity is the N-terminal HIS-Tag, which might act as a sterical obstacle. Moreover, GAPDH proteins form catalytically active homotetramers as well as heterotetramers (McAlister and Holland, 1985). Misfolded proteins, for instance, could negatively affect this tetrameric formation. Another possibility for the observed higher activity of GAPDH in wild type might be that there is much more protein in the cell, than actually required. This would also explain the comparable growth rates of the *klaGAPDH* mutant and the wild type.

In glucose minimal medium batch cultures the glucose uptake rate, the ethanol- and acetate exretion rates were lower, presumably caused by the slightly slower growth. The ethanol formation per consumed glucose ratio was lower as well. This result points out that already the *klaGAPDH* mutant, to a small extent, shows the intended effect of switching from ethanol towards TAG production. On the other hand, the glycerol excretion rate as well as the glycerol per glucose ratio was increased. One major function of glycerol synthesis in the cell is to maintain the redox balance. The conversion of the glycolytic intermediate DHAP into glycerol-3-phosphate by G3PD reoxidizes NADH, produced by glycolysis. This might be particularly important for respirofermentative growth in the presence of glucose (Ansell et al., 1997). However, the klaGAPDH activity should lower cytosolic NADH amounts and increase NADPH. In response to a decreased NADH concentration in the cytosol, a lower glycerol production in the cell would have been expected. Another major cytosolic NADH producing pathway represents amino acid synthesis. Especially in minimal medium the cell has to *de novo* synthesize amino acids from glucose and ammonia, which might lead to an excess of NADH (Albers et al., 1996). Another explanation for the higher glycerol production might be that the low klaGAPDH activity acts as a bottleneck in glycolysis and glycerol formation represents a valve.

However, this putative bottleneck and the resulting decreased glycolytic carbon flux did probably not affect lipid synthesis. The 1.4−fold increase of TAG compared to the wild type is most likely caused by a higher cytosolic NADPH concentration.

5.2. *klaGAPDH UTR1* mutant

The GPD1 UTR1 mutant showed a severe growth defect under nitrogen starved conditions, whereas the growth in glucose batch cultures did not show such a strong phenotype.

Furthermore, the TAG content dropped dramatically compared to the *klaGAPDH* mutant and even to wild type. One suggestion is that the *TDH2* locus simply was not the right choice for the *UTR1opt* integration. A very low expression even in exponential phase of the NAD(H)-kinase was determined, although *UTR1opt* was overexpressed by a strong promotor (truncated HXT7 promotor). There are several suggestions which could explain this low expression level. First, the mRNA translation of the NAD(H)-kinase might not be effective enough, although the codon usage bias was optimized for *S. cerevisiae*. This should on the one hand prolong the half-life of the mRNA (Presnyak et al., 2015) and on the other hand result in the use of preferred codons, which show high concentrations of their corresponding tRNAs in the cytosol. The poor NAD(H)-kinase yield might also be related to structural or sequence elements, that contribute to a faster decay of the transcript, such as 5' and 3' untranslated regions or the tendency of the poly(A) tail to build a double-stranded structure (Geisberg et al., 2014).

The second suggestion refers to a possible protein instability of the NAD(H)-kinase. For instance, misfolded and damaged proteins get degraded to avoid toxicity in the cell (Schrader, Harstad, and Matouschek, 2009). However, a plasmid expressed NAD(H)-kinase was analyzed as well and showed an expression similar to klaGAPDH (data not shown). The *UTR1opt* was encoded by a high copy number plasmid. This high plasmid concentration in the cell and a constant expression of *UTR1opt* might have masked its protein instability. Nevertheless, another effect on protein stability might have a negative feedback mechanism resulting in response to an increased cytosolic NADPH concentration (caused by klaGAPDH). Besides that, it is interesting, that the genome-integrated *UTR1opt* of the *klaGAPDH UTR1 adh1*Δ shows higher expression levels again. Somehow the *ADH1* deletion seems to stabilize the protein (see section 5.3).

However, there will be more studies necessary to get viable results regarding this strain.

5.3. *klaGAPDH UTR1 adh1*Δ mutant

The most prominent phenotype of the *klaGAPDH UTR1 adh1*Δ mutant was its very slow growth. Due to the Crabtree effect *ADH1* represents one of the most actively transcribed genes of *S. cerevisiae*. This phenomenon describes the unique behavior of *S. cerevisiae*, where even under aerobic conditions the yeast produces ethanol rather than forming biomass via the TCA cycle.

The *klaGAPDH UTR1 adh1*Δ mutant excreted high amounts of glycerol in both media (C-lim and N-lim). It seems that the mutant had to respond to redox imbalances caused by the *ADH1* deletion. The fermentation of glucose to ethanol is achieved by decarboxylation of the glycolysis product pyruvate to acetaldehyde, which is further reduced to ethanol by the alcohol dehydrogenase (gene product of *ADH1*) and by oxidation of NADH to NAD^+.

Therefore, one major pathway, which enables the cell to maintain its redox balance, is missing. This might be compensated by glycerol snythesis.

Cronwright, Rohwer, and Prior, 2002, constructed a kinetic model of the glycerol synthesis pathway and found that DHAP has more influence on the glycerol flux than NADH (response coefficients of 0.48 to 0.69 and 0.03 to 0.08, respectively). They assumed that this is most likely due to the higher affinity of G3PD for NADH than for DHAP. The intracellular concentrations of NADH are high enough to ensure a saturation of all G3PD proteins. Therefore, an increase of NADH would not affect G3PD activity anymore. Taking this into account leads to the assumption that due to the cells inability of ethanol production and a concomitant carbon flux stagnation, a feedback mechanism might get active which leads to an accumulation of DHAP. Gruning et al., 2014, for instance found that TPI, which converts DHAP to GAP, is inhibited by the pyruvate kinase substrate phosphoenolpyruvat (PEP). This results in a higher DHAP concentration which in turn triggers G3PD acitivity (Cronwright, Rohwer, and Prior, 2002).

The performed western blot showed a higher expression of the NAD(H)-kinase in the *klaGAPDH UTR1 adh1*Δ mutant. This is most likely due to oxidative stress as the cell might need to switch to aerobic respiration in order to produce enough ATP for fatty acid synthesis. As DHAP is used for glycerol formation, two ATP-forming steps of glycolysis are missing (1,3BPG to 3PG and PEP to pyruvate). Interestingly, the TAG contents of the mutant and the wild type were similar. In contrast to ethanol and glycerol production, fatty acid synthesis requires ATP. The above described loss of ATP via glycerol formation might be compensated by ATP Production via aerobic respiration (oxidative phosphorylation). As a consequence of aerobic respiration the cell has to cope with oxidative stress. It is known that NADPH represents the redox cofactor for antioxidant neutralizing enzymes and is crucial for glutathion synthesis (Outten, 2003, Pollak, Dölle, and Ziegler, 2007). The cellular oxidative stress response might somehow trigger the expression of NAD(H)-kinase in order to produce NADPH.

Another suggestion for the observed expression levels of NAD(H)-kinase again refers to its stability. As already mentioned the *ADH1* deletion seems to stabilize the protein. This might be due to a lower cytosolic NADPH concentration, caused by the glycolytic arrest, which would repress a putative negative feedback loop, as already discussed in section 5.2.

Generally, the *ADH1* deletion might force the cell to produce energy via aerobic respiration, which further leads to oxidative stress. Besides that, the cell is most likely not able to balance its redox equivalents, due to the inability of ethanol production, which results in a high glycerol excretion rate. Moreover, the *ADH1* deletion might cause a stagnation of glycolysis, which affects glycerol production as well. Nevertheless, in contrast to the double mutant *klaGAPDH UTR1*, this triple mutant is able to accumulate TAG amounts per dry weight similar to wild type.

5.4. *HXT1* mutant

The *HXT1* mutant was engineered to increase the glycolytic flux in the cell during nitrogen starved conditions. In C-lim the glucose uptake rates of wild type and mutant are similar. Even though the *HXT1mut* is overexpressed, which was also observed by western blot and microscopy, no difference in exponential phase, when both strains expressed Hxt1p at high levels, was detected. Paying attention to the microscopy figures, two organelles showed fluorescence: the vacuole and the cell membrane. During the exponential phase a brighter fluorescence in the cell membrane than in the vacuole was expected. Vacuolar signals often represent degradation products of GFP-constructs. The observed vacuolar signal might be caused by the dynamics of exponential phase, where proteins are constantly being degraded and resynthesized. The overexpression of *HXT1mut* might have amplified this dynamic system, causing accumulation of GFP in the vacuole. The vacuolar GFP, as a putative degradation product ($\approx 26kD$), was also detected by western blot.

Comparing the microscopic figures of stationary phase with those of exponential phase, it can be seen that the *HXT1* mutant cells lost their intense signal in the vacuole, but showed a similarly bright signal in the cell membrane. The *HXT1wt* was already completely degraded, only a weak signal in the vacuole was observed. This signal is most likely derived from the remaining GFP, as it is known to be very stable in the cell (Corish and Tyler-Smith, 1999). *HXT1mut* is controlled by the strong *PGK1* promotor, which prevents repression by Rgt1p when glucose is limited (Mosley et al., 2003). In stationary phase, the glucose in the medium is already consumed, which leads to the repression of *HXT1* transcription in wild type cells (Polish, 2005). In contrast, the mutant's expression does not depend on the external glucose concentration (Partow et al., 2010), but on general signaling pathways when cells enter stationary phase (Herman, 2002). The metabolism of the mutant slows down and the mutation of the protein prevents its degradation. This leads to a prolonged stay of the mutated Hxt1p in the cell membrane, which explains the weak signal in the vacuole as less degradation product accumulates.

Microscopic and expression studies showed clear results. The wild type Hxt1p was degraded already after 24 hours of nitrogen starvation, whereas the mutant Hxt1p still showed a solid expression after 48 hours. The microscopic figures showed bright signals in the vacuole of the mutant. Therefore, the degradation of the mutant Hxt1p takes place and GFP accumulates, whicht might be due to the overexpression. Nevertheless, a cell membrane location is still detectable, but it is not clear if this is caused by the overexpression or by preventing the protein from degradation.

6. Conclusion

The obtained results regarding the redox-reprogrammed mutants lead to two possible conclusions:

First, the intended effect of turning the Crabtree effect into an advantage by switching from ethanol to TAG production, without the need of aerobic respiration, worked at least to a small extent in the *klaGAPDH* mutant. This mutant already produced less ethanol and more lipid. Some of the carbon source got lost by glycerol formation, in order to maintain the redox balance. Assuming a decrease of the glycolytic flux rate, glycerol formation also might act as a valve to prevent accumulation of glycolytic imtermediates. A similar effect was shown by the triple mutant *klaGAPDH UTR1 adh1*Δ. Moreover, it showed a higher TAG content than observed in the double mutant *klaGAPDH UTR1*, which synthesized only very low amounts of TAG. Therefore, engineering a double mutant *klaGAPDH adh1*Δ might become a future task. To avoid glycerol formation, it would be interesting to examine the effect of deleting *GPD1*, the gene which encodes for G3PD. This deletion might be lethal, as the cell probably loses its ability to maintain the redox balance or counterbalancing a possible glycolytic flux stagnation. On the other hand, the deletion might be beneficial for TAG production, as the carbon source used for glycerol formation, possibly gets redirected towards TAG synthesis.

Second, the cells are partially switching to aerobic respiration in order to produce enough ATP for fatty acid synthesis, as one part of the ATP-producing steps during glycolysis gets lost due to glycerol formation. High biomass and lipid amounts are mostly coupled to aerobic respiration, which is particularly true for oleaginous yeasts (Kolouchová et al., 2016). The Crabtree effect instead relies on an overflow metabolism, which means an incomplete oxidation of carbon sources (glucose) by excreting, for instance, ethanol (Urk et al., 1989). Oleaginous yeasts are able to store carbon sources in the form of TAG. The highly efficient ATP production via oxidative phosphorylation might be important for the storage of carbon sources within lipid, hence, biomass formation. However, this hypothesis can only be confirmed by performing anaerobic batch culture experiments.

The results obtained by analyzing the *HXT1* mutant led to the conclusion that the Hxt1p mutation has to be combined with a deletion of *GSY1* and *GSY2*. These genes encode the enzyme glycogen synthase. Most of the additional glucose is directly stored within glycogen. By deleting these gene the glucose might enter glycoslysis and might further be available for TAG synthesis.

7. Summary and Outlook

Yeasts represent promising microbial factories for lipid production. Wild type yeast strains produce a similar pattern of lipids as plants, which are used for biodiesel production. This makes yeast lipids a potential raw material for the production of the so called second and third generation biodiesel (Papanikolaou and Aggelis, 2011). Moreover, yeasts can achieve higher growth rates and higher biomass production than algae, which in turn allows higher biodiesel productivities (Bellou et al., 2014, Fakas, 2016).

For this reason and to obtain an optimal fermentation, metabolic engineering is required. *S. cerevisiae* represents a well studied model organism, which facilitates genetic modifications. Furthermore, the profound knowledge about the regulation of various metabolic pathways and the involved key genes makes it easier to modify and reprogram its metabolism towards TAG production. The metabolic interventions, which were performed in the course of this thesis, are based on this knowledge.

First, the integration of the klaGAPDH was carried out, whereby a shift towards cytosolic NADPH production was achieved. NADPH represents the cofactor for the reduction steps in fatty acid biosynthesis. A higher availability of this cofactor therefore might trigger TAG production. Indeed, the TAG content of the *klaGAPDH* mutant increased by 1.4-fold, in comparison to the wild type. Next, to increase the low $NADP^+/NAD^+$ ratio in the cytosol of the cell, the overexpression of *UTR1opt* was performed (Pollak, Dölle, and Ziegler, 2007). *UTR1opt* phosphorylates cytosolic NAD^+, which can be further utilized by klaGAPDH. The TAG content of this mutant dropped tremendously for unknown reasons.

Finally, *ADH1* was deleted, whereby a total redirection of the glycolytic carbon resources from ethanol towards TAG production was intended. The resulting strain excretes high amounts of glycerol, probably caused by the cells redox imbalance and a glycolytic flux stagnation. Moreover this strain probably has to cope with oxidative stress, which utilizes NADPH instead of using it for TAG synthesis. Although, these metabolic effects resulted in a severe growth defect, the strain accumulates similar TAG amounts per dry weight as the wild type.

The second part of the thesis implied increasing the glycolytic flux under nitrogen starvation by a mutated Hxt1p. It was found that the mutated transporter got degraded less quickly under nitrogen starved conditions than the wild type transporter, which positively

affected glucose consumption. The TAG content and the secreted metabolite concentrations showed no difference referring to those of wild type. Glycogen instead increased (25%). The additionally consumed glucose therefore got stored within glycogen.

In order to be competitive with oleaginous yeasts it will be crucial to combine advantageous metabolic interventions in one strain. The integration of *UTR1opt* has to occur into another target locus and the deletion of *ADH1* has to be further evaluated concerning the cells growth defect.

The final target strain already bears several mutations beneficial for TAG accumulation, for instance deletions of the genes encoding TAG degrading enzymes (*TGL3, TGL4*). Metabolic pathways which compete with TAG for carbon resources are deleted as well. Especially the deletion of the glycogen synthase genes (*GSY1, GSY2*) is important in combination with the mutated *HXT1*. Moreover, a hyperactive acetyl-CoA carboxylase 1 (ACC1 S1157A A1257S, Hofbauer et al., 2014), which catalyzes the first step of fatty acid synthesis (carboxylation of acetyl-CoA to malonyl-CoA) is expressed in this strain. Many more engineering steps are in progress, for instance, redirecting the carbon sources from cell wall glucan towards TAG or increasing the lipid droplet size of *S. cerevisiae*.

The future aim is to get rid of ethanol production and its concomitant loss of carbon by converting the Crabtree effect into an advantage. This may result in a strain producing similar lipid yields as oleaginous yeasts but without the need of high aeration rates for respiration.

Appendix A.

Materials

Table A.1.: Yeast extract-peptone-dextrose complex medium **(YPD)**

Glucose mono hydrate	22 g L^{-1}
Yeast extract	10 g L^{-1}
Peptone	20 g L^{-1}

YPD agar plates were prepared by adding 20 g L^{-1} of agar before autoclaving. For selection plates either 100 mg L^{-1} of nourseothricin sulfate (clonNAT) or 50 mg L^{-1} of geneticin (G418) were added. The plates were stored at 4 °C.

Table A.2.: Carbon limited minimal medium **(C-lim)**

Glucose monohydrate	22 g L^{-1}
Potassium dihydrogen phosphate	3 g L^{-1}
Magnesium sulfate heptahydrate	0.5 g L^{-1}
Ammonium sulfate heptahydrate	4 g L^{-1}
Phthalat (0.5 M)	40 ml/l
Delft vitamin stock solution (1000x)	1 mL L^{-1}
Delft trace elements stock solution (1000x)	1 mL L^{-1}
Inositol (1000x)	1 mL L^{-1}
Ampicillin	100 μg L^{-1}

Table A.3.: Nitrogen limited minimal medium **(N-lim)**

Glucose monohydrate	22 g L^{-1}
Potassium dihydrogen phosphate	3 g L^{-1}
Magnesium sulfate heptahydrate	0.5 g L^{-1}
Ammonium sulfate heptahydrate	0.2 g L^{-1}
Phthalat (0.5 M)	40 mL L^{-1}
Delft vitamin stock solution (1000x)	1 mL L^{-1}
Delft trace elements stock solution (1000x)	1 ml L^{-1}
Inositol (1000x)	1 ml L^{-1}
Ampicillin	100 μg L^{-1}

Glucose was autoclaved separately from potassium dihydrogen phosphate, magnesium sulfate heptahydrate and ammonium sulfate heptahydrate. The pH of C-lim was set to 5.5 using 1 M KOH, whereas the pH of N-lim was set to 4 using 1 M HCl. After cooling down from autoclaving all components were mixed.

Table A.4.: **Delft vitamin stock solution** (1000x)

Biotin	0.05 g L^{-1}
Calcium d-pantothenate	1 g L^{-1}
Niacin	1 g L^{-1}
Inositol	25 g L^{-1}
Thiamine hydrochloride	1 g L^{-1}
Pyridoxal hydrochloride	1 g L^{-1}
Benzoic acid	0.2 g L^{-1}

Table A.5.: **Delft trace elements stock solution** (1000x)

EDTA	15 g L^{-1}
Zinc sulfate heptahydrate	4.5 g L^{-1}
Manganese chloride tetrathydrate	0.8 g L^{-1}
Cobalt chloride hexahydrate	0.3 g L^{-1}
Copper sulfate pentahydrate	0.3 g L^{-1}
Sodium molybdate dihydrate	0.4 g L^{-1}
Calcium chloride·dihydrate	4.5 g L^{-1}
Ferric sulfate heptahydrate	3 g L^{-1}
Boric acid	1 g L^{-1}
Potassium iodid	0.1 g L^{-1}

Delft vitamin stock solution (1000x) and trace elements stock solution (1000x) were sterile filtrated and stored at 4 °C.

Table A.6.: **Chemical list**

Chemical	**Company**	**Cat.nr**
Acetic acid (glacial)	Merck	1.00063.2511
Acetone	Roth	7328.2
Acetonitril	J.T.	Baker 9017
Acrylamid 30%	Bio-Rad	161-6156
Acrylamid 40%	Bio-Rad	161-0148
Agarose	Biozyme	840004
Ammonium acetate	Fluka	9689
Ammonium persulfate	Bio-Rad	161-0700
Ammonium sulfate	Roth	3746.1
Amyloglucosidase	Sigma	-
Antipain	Sigma Aldrich	12880
Benzoic acid	Sigma Aldrich	B3250
Biotin	Merck	5.00030.0010
Boric acid	Merck	1.00165
Calcium chloride dihydrate	Fluka	21097
Calcium d-pantothenate	Sigma-Aldrich	PHR1232

Chemical	**Company**	**Cat.nr**
Chemilumiscence substrate	Thermo Scientific	OA182377
Chloroform	Sigma Aldrich	34854
Cholesteryl palmitate	Sigma Aldrich	C6072
Cobalt chloride hexahydrate	Sigma	C2644
Copper sulfate pentahydrate	Merck	2790
ddH_20	LiChrosolv	1.15333.1000
Dithiothreitol	Roche	DTT-RO
D-Sorbit	Roth	6.284 892
EDTA	Merck	1.08418.1000
Ergosterol	Acros Organics	117810050
Ferric sulfate heptahydrate	-	-
Glass beads	Sartorius	BBI-8541701
Glucose monohydrate	Roth	6887.2
Glutamic acid	Sigma Aldrich	G1251
Glycine	AppliChem	A1067, 5000
Inositol	Aldrich	87-89-8
Isopropanol	Roth	7343.1
Leupeptin	Sgma Aldrich	-
Lithium acetate	Aldrich	517992
Magnesium chloride	Merck	906 A376433
Magnesium sulfate	Roth	P027.1
Manganese chloride	-	-
MES hydrate	Sigma Aldrich	M2933
Methanol	J.T. Baker	8045
Micro Amp 96 well plates	Applied Biosystems	4346906
NAD^+	Roche	NAD100-RO
$NADP^+$	Roche	NADP-RO
Niacin	Fluka	72310
PEG 4000	USP	1546569
Pepstatin A	Sigma Aldrich	-
Peptone	BD	211820
Phenol–chloroform–isoamyl alcohol mixture	Sigma Aldrich	-
Phosphoric acid	Merck	573
Phthalic acid	Sigma Aldrich	P39303
Potassium chloride	Sigma Aldrich	1.04936
Potassium dihydrogen phosphate	Roth	3904.1
Potassium iodid	Vetec	V000130
Pyridoxal hydrochloride	Calbiochem	545060
SDS	Sigma Aldrich	L3771
Sodium chloride	Roth	3957.1
Sodium hydroxide	Merck	6498

Chemical	**Company**	**Cat.nr**
Sodium molybdate dihydrate	-	-
Sodium phospate	Aldrich	342483
Sulphuric acid	-	-
TEMED	Roth	2367.3
Tergitol	Sigma Aldrich	NP40S
Thiamine hydrochloride	Sigma Aldrich	T-4625
Triacylglycerol 48:3	Larodan	33-1610-12
Trichloroacetic acid	Merck	1.00807.1000
Triethanolamin	Merck	1.08379.1000
Triton X-100	Sigma Aldrich	T-8787
Tris	Roth	4855.3
Tween 20	Merck	8.22184.0500
Water	in-house distillery	-
Yeast extract	BD	212720
Zinc sulfate	Roth	K301.1

Bibliography

Albers, E et al. (Sept. 1996). "Influence of the nitrogen source on Saccharomyces cerevisiae anaerobic growth and product formation." In: *Applied and environmental microbiology* 62 (9), pp. 3187–3195. ISSN: 0099-2240 (cit. on pp. 26, 44).

Albery, W. John and Jeremy R. Knowles (Dec. 1976). "Free-energy profile for the reaction catalyzed by triosephosphate isomerase." In: *Biochemistry* 15.25, pp. 5627–5631. DOI: 10.1021/bi00670a031 (cit. on p. 34).

Ansell, Ricky et al. (May 1997). "The two isoenzymes for yeast NAD-dependent glycerol 3-phosphate dehydrogenase encoded byGPD1andGPD2have distinct roles in osmoadaptation and redox regulation." In: *The EMBO Journal* 16.9, pp. 2179–2187. DOI: 10.1093/emboj/16.9.2179 (cit. on p. 44).

Bellou, Stamatia et al. (Dec. 2014). "Microalgal lipids biochemistry and biotechnological perspectives." In: *Biotechnology Advances* 32.8, pp. 1476–1493. DOI: 10.1016/j.biotechadv.2014.10.003 (cit. on p. 49).

Christen, Stefan and Uwe Sauer (Jan. 2011). "Intracellular characterization of aerobic glucose metabolism in seven yeast species by 13C flux analysis and metabolomics." In: *FEMS Yeast Research* 11.3. uptake secretion rates, pp. 263–272. DOI: 10.1111/j.1567-1364.2010.00713.x (cit. on p. 23).

Corish, Pete and Chris Tyler-Smith (Dec. 1999). "Attenuation of green fluorescent protein half-life in mammalian cells." In: *Protein Engineering, Design and Selection* 12.12, pp. 1035–1040. DOI: 10.1093/protein/12.12.1035 (cit. on p. 47).

Cronwright, G. R., J. M. Rohwer, and B. A. Prior (Sept. 2002). "Metabolic Control Analysis of Glycerol Synthesis in Saccharomyces cerevisiae." In: *Applied and Environmental Microbiology* 68.9, pp. 4448–4456. DOI: 10.1128/aem.68.9.4448-4456.2002 (cit. on p. 46).

Delgado, M. Luisa et al. (Feb. 2001). "The glyceraldehyde-3-phosphate dehydrogenase polypeptides encoded by the Saccharomyces cerevisiae TDH1, TDH2 and TDH3 genes are also cell wall proteins." In: *Microbiology* 147.2, pp. 411–417. DOI: 10.1099/00221287-147-2-411 (cit. on p. 43).

Fakas, Stylianos (July 2016). "Lipid biosynthesis in yeasts: A comparison of the lipid biosynthetic pathway between the model nonoleaginous yeastSaccharomyces cerevisiaeand the model oleaginous yeastYarrowia lipolytica." In: *Engineering in Life Sciences* 17.3, pp. 292–302. DOI: 10.1002/elsc.201600040 (cit. on pp. 1, 49).

Geisberg, Joseph V. et al. (Feb. 2014). "Global Analysis of mRNA Isoform Half-Lives Reveals Stabilizing and Destabilizing Elements in Yeast." In: *Cell* 156.4, pp. 812–824. DOI: 10.1016/j.cell.2013.12.026 (cit. on p. 45).

Gruning, N.-M. et al. (Mar. 2014). "Inhibition of triosephosphate isomerase by phosphoenolpyruvate in the feedback-regulation of glycolysis." In: *Open Biology* 4.3, pp. 130232–130232. DOI: 10.1098/rsob.130232 (cit. on p. 46).

Harris, Thomas K. et al. (Nov. 1998). "Proton Transfer in the Mechanism of Triosephosphate Isomerase†." In: *Biochemistry* 37.47, pp. 16828–16838. DOI: 10.1021/bi982089f (cit. on p. 34).

Herman, Paul K (Dec. 2002). "Stationary phase in yeast." In: *Current Opinion in Microbiology* 5.6, pp. 602–607. DOI: 10.1016/s1369-5274(02)00377-6 (cit. on p. 47).

Hofbauer, Harald F. et al. (June 2014). "Regulation of Gene Expression through a Transcriptional Repressor that Senses Acyl-Chain Length in Membrane Phospholipids." In: *Developmental Cell* 29.6, pp. 729–739. DOI: 10.1016/j.devcel.2014.04.025 (cit. on p. 50).

Kawai, Shigeyuki et al. (June 2001). "Molecular cloning and identification ofUTR1of a yeastSaccharomyces cerevisiaeas a gene encoding an NAD kinase." In: *FEMS Microbiology Letters* 200.2, pp. 181–184. DOI: 10.1111/j.1574-6968.2001.tb10712.x (cit. on p. 3).

Knothe, Gerhard (June 2010). "Biodiesel and renewable diesel: A comparison." In: *Progress in Energy and Combustion Science* 36.3, pp. 364–373. DOI: 10.1016/j.pecs.2009.11.004 (cit. on p. 1).

Kolouchová, Irena et al. (Mar. 2016). "Lipid accumulation by oleaginous and non-oleaginous yeast strains in nitrogen and phosphate limitation." In: *Folia Microbiologica* 61.5, pp. 431–438. DOI: 10.1007/s12223-016-0454-y (cit. on pp. 4, 26, 48).

McAlister, Lee and Michael J. Holland (1985). "Differential expression of the three yeast glyceraldehyde-3-phosphate dehydrogenase genes." In: (cit. on pp. 43, 44).

Mosley, Amber L. et al. (Jan. 2003). "Glucose-mediated Phosphorylation Converts the Transcription Factor Rgt1 from a Repressor to an Activator." In: *Journal of Biological Chemistry* 278.12, pp. 10322–10327. DOI: 10.1074/jbc.m212802200 (cit. on p. 47).

Nijland, Jeroen G. et al. (July 2016). "Improving pentose fermentation by preventing ubiquitination of hexose transporters in Saccharomyces cerevisiae." In: *Biotechnology for Biofuels* 9.1. DOI: 10.1186/s13068-016-0573-3 (cit. on p. 4).

Outten, C. E. (May 2003). "A novel NADH kinase is the mitochondrial source of NADPH in Saccharomyces cerevisiae." In: *The EMBO Journal* 22.9, pp. 2015–2024. DOI: 10.1093/emboj/cdg211 (cit. on p. 46).

Papanikolaou, Seraphim and George Aggelis (June 2011). "Lipids of oleaginous yeasts. Part II: Technology and potential applications." In: *European Journal of Lipid Science and Technology* 113.8, pp. 1052–1073. DOI: 10.1002/ejlt.201100015 (cit. on p. 49).

Parks, Leo W. and Warren M. Casey (Oct. 1995). "Physiological Implications of Sterol Biosynthesis in Yeast." In: *Annual Review of Microbiology* 49.1, pp. 95–116. DOI: 10.1146/annurev.mi.49.100195.000523 (cit. on pp. 25, 26).

Partow, Siavash et al. (Nov. 2010). "Characterization of different promoters for designing a new expression vector in Saccharomyces cerevisiae." In: *Yeast* 27.11, pp. 955–964. DOI: 10.1002/yea.1806 (cit. on p. 47).

Polish, J. A. (Feb. 2005). "How the Rgt1 Transcription Factor of Saccharomyces cerevisiae Is Regulated by Glucose." In: *Genetics* 169.2, pp. 583–594. DOI: 10.1534/genetics.104.034512 (cit. on p. 47).

Pollak, Nadine, Christian Dölle, and Mathias Ziegler (Mar. 2007). "The power to reduce: pyridine nucleotides small molecules with a multitude of functions." In: *Biochemical Journal* 402.2, pp. 205–218. DOI: 10.1042/bj20061638 (cit. on pp. 46, 49).

Presnyak, Vladimir et al. (Mar. 2015). "Codon Optimality Is a Major Determinant of mRNA Stability." In: *Cell* 160.6, pp. 1111–1124. DOI: 10.1016/j.cell.2015.02.029 (cit. on p. 45).

Ran, F. Ann et al. (Sept. 2013). "Double Nicking by RNA-Guided CRISPR Cas9 for Enhanced Genome Editing Specificity." In: *Cell* 154.6, pp. 1380–1389. DOI: 10.1016/j.cell.2013.08.021 (cit. on p. 7).

Rose, Irwin A., Wen Jian Fung, and Jessie V. B. Warms (May 1990). "Proton diffusion in the active site of triosephosphate isomerase." In: *Biochemistry* 29.18, pp. 4312–4317. DOI: 10.1021/bi00470a008 (cit. on p. 34).

Roy, Adhiraj et al. (Sept. 2014). "Glucose starvation-induced turnover of the yeast glucose transporter Hxt1." In: *Biochimica et Biophysica Acta (BBA) - General Subjects* 1840.9, pp. 2878–2885. DOI: 10.1016/j.bbagen.2014.05.004 (cit. on p. 15).

Rozovsky, S. and A. E. McDermott (Feb. 2007). "Substrate product equilibrium on a reversible enzyme, triosephosphate isomerase." In: *Proceedings of the National Academy of Sciences* 104.7, pp. 2080–2085. DOI: 10.1073/pnas.0608876104 (cit. on p. 34).

Schrader, Erin K, Kristine G Harstad, and Andreas Matouschek (Nov. 2009). "Targeting proteins for degradation." In: *Nature Chemical Biology* 5.11, pp. 815–822. DOI: 10.1038/nchembio.250 (cit. on p. 45).

Tehlivets, Oksana, Kim Scheuringer, and Sepp D. Kohlwein (Mar. 2007). "Fatty acid synthesis and elongation in yeast." In: *Biochimica et Biophysica Acta (BBA) - Molecular and Cell Biology of Lipids* 1771.3, pp. 255–270. DOI: 10.1016/j.bbalip.2006.07.004 (cit. on p. 2).

Urk, H. Van et al. (Sept. 1989). "Glucose Transport in Crabtree-positive and Crabtree-negative Yeasts." In: *Microbiology* 135.9, pp. 2399–2406. DOI: 10.1099/00221287-135-9-2399 (cit. on p. 48).

Verho, Ritva et al. (Nov. 2002). "Identification of the First Fungal NADP-GAPDH fromKluyveromyces lactis†." In: *Biochemistry* 41.46, pp. 13833–13838. DOI: 10.1021/bi0265325 (cit. on pp. 3, 20, 33).

Wiebe, Marilyn G. et al. (Feb. 2008). "Central carbon metabolism ofSaccharomyces cerevisiaein anaerobic, oxygen-limited and fully aerobic steady-state conditions and

following a shift to anaerobic conditions." In: *FEMS Yeast Research* 8.1, pp. 140–154. DOI: 10.1111/j.1567-1364.2007.00234.x (cit. on p. 2).

Wolinski, Heimo and Sepp D. Kohlwein (2015). "Microscopic and Spectroscopic Techniques to Investigate Lipid Droplet Formation and Turnover in Yeast." In: *Membrane Trafficking: Second Edition*. Ed. by Bor Luen Tang. New York, NY: Springer New York, pp. 289–305. ISBN: 978-1-4939-2309-0. DOI: 10.1007/978-1-4939-2309-0_21. URL: https://doi.org/10.1007/978-1-4939-2309-0_21 (cit. on p. 22).

Yang, H. et al. (May 1996). "Sterol Esterification in Yeast: A Two-Gene Process." In: *Science* 272.5266, pp. 1353–1356. DOI: 10.1126/science.272.5266.1353 (cit. on p. 25).

Yen, Hong-Wei and Yi Xian Liu (Aug. 2014). "Application of airlift bioreactor for the cultivation of aerobic oleaginous yeast Rhodotorula glutinis with different aeration rates." In: *Journal of Bioscience and Bioengineering* 118.2, pp. 195–198. DOI: 10.1016/j.jbiosc.2014.01.002 (cit. on p. 1).

Zhang, Fuzhong, Sarah Rodriguez, and Jay D Keasling (Dec. 2011). "Metabolic engineering of microbial pathways for advanced biofuels production." In: *Current Opinion in Biotechnology* 22.6, pp. 775–783. DOI: 10.1016/j.copbio.2011.04.024 (cit. on p. 1).